Suspended extrusion-based bioprinting to establish a 3D *in vitro* model of a neural network to study Parkinson's disease

---

Major Research Project Report
by
Dieuwke de Vos
5593352
Master of Regenerative Medicine and Technology
University of Utrecht
03 March 2022

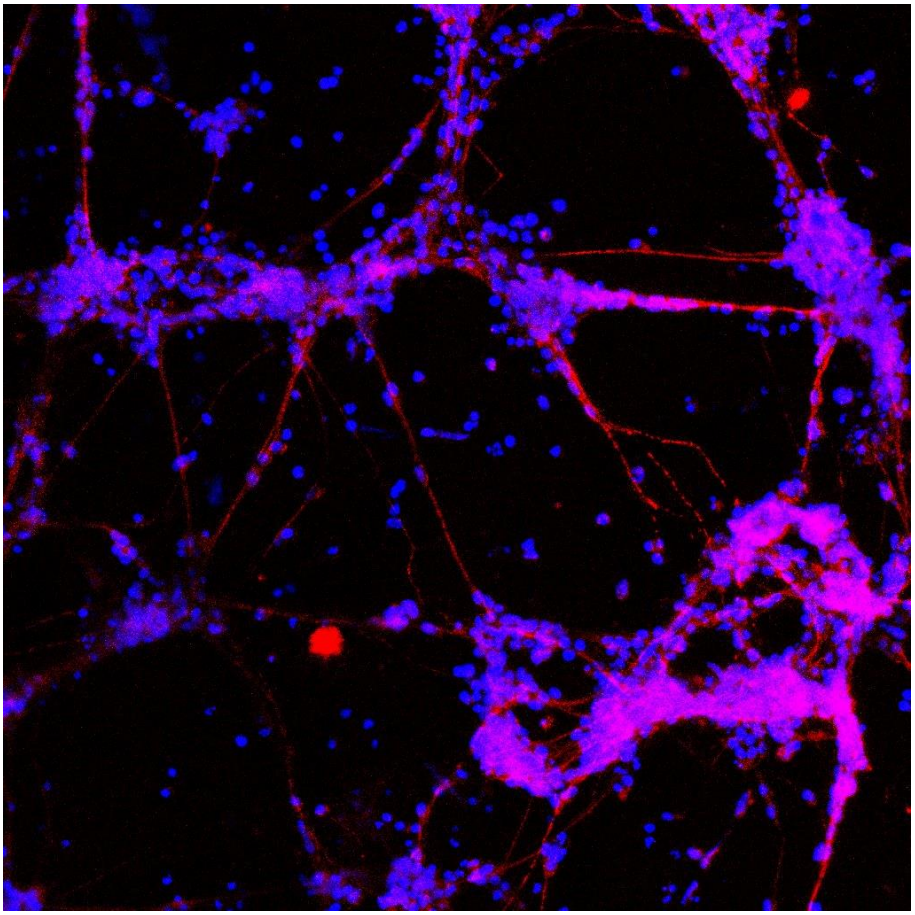

Universiteit Utrecht

UMC Utrecht

Table of Contents

Abstract **2**
Layman's Summary **3**
1. Introduction **4**
2. Materials and Methods **7**
2.1 Preparation and analysis of milled GelMA suspension baths **7**
2.1.1 Preparation of milled GelMA suspension bath 7
2.1.2 Microparticle size 7
2.1.3 Mechanical Testing 7
2.1.4 Swelling Ratio and Sol Fraction 8
2.2 Cell Culture **8**
2.2.1 hiMSC 8
2.2.2 hESC 8
2.2.3 LUHMES 9
2.3 3D bioprinting process **9**
2.3.1 Printing hiMSC **10**
2.3.2 Printing hESC 10
2.3.3 Printing LUHMES 10
2.4 Cell Viability Assays to determine Printing Resolution and Filament Width **11**
2.5 Neuronal Differentiation Studies using Immunocytochemistry **12**
2.5.1 LUHMES suspension – biomaterials 12
2.5.2 LUHMES suspension - cell densities 13
2.5.3 LUHMES print 13
2.6 Statistics **13**
3. Results and Discussion **14**
3.1 Preparation and characterization of milled GelMA suspension bath **14**
3.1.1 Preparation of milled GelMA suspension bath 14
3.1.2 Milling for 60s results in the optimal microparticle slurry 14
3.1.3 Milling for 60s results in mechanical stiffness <20 kPa 16
3.1.4 Swelling Properties of 5% milled and bulk GelMA are comparable 17
3.2 3D print parameters **18**
3.3 3D bioprinting process **18**
3.3.1 Printing hiMSC at low pressure results in good cell viability 18
3.3.2 Printing hESC at low pressure results in good resolution and high cell viability 20
3.3.3 LUHMES cells printed in a gelatin bioink at high cell density form aggregates 21
3.4 Neuronal Differentiation Studies using Immunocytochemistry **23**
3.4.1 LUHMES cells in milled GelMA suspensions with Matrigel and Fibronectin form neurites 23
3.4.2 LUHMES cells in milled GelMA suspensions form neurites at different cell densities 24
3.5 LUHMES print **25**
3.5.1 Bioprinting of LUHMES results in high cell viability 25
3.5.2 Bioprinted LUHMES cells form neurites in 3D 27
4. Conclusions **29**
5. Future Outlook **30**
Acknowledgements **31**
References **32**
Supplementary Figures **37**
Appendix **40**

Abstract

Parkinson's disease (PD) is a common neurodegenerative disorder that affects a rapidly increasing number of patients worldwide. However, current PD models, including 2D *in vitro* cultures and animal models, either lack the three-dimensional (3D) cell-cell interactions and complexity of the native brain microenvironment or are not comprised of human cells. To better replicate *in vivo* brain tissue, biofabrication can be employed, which enables precise deposition of biomaterials and cells to create more complex *in vitro* models. This study describes a new strategy to develop a 3D *in vitro* model comprising a neural network by suspended extrusion-based bioprinting of a cell-laden bioink to build a construct in a layer-by-layer fashion to permit omnidirectional growth of neurons. In order to reach this goal, a novel, photo-crosslinkable suspension bath of highly tunable mechanical properties was developed and characterized, using gelatin methacryloyl (GelMA) microparticles to act as a Bingham plastic. In this bioresin, soft, cell-laden bioinks were embedded, employing first human immortalized (hiMSCs), secondly human embryonic stem cells (hESCs), and lastly, neural cells, which were differentiated into neurons to form a 3D neural network. The results of this project show that milling 5% GelMA for 60s results in a suspension bath of low mechanical stiffness, which is suitable for printing hiMSC at a high cell viability and shape fidelity, and hESCs at a high cell viability and resolution of 400 µm. Moreover, they demonstrate that suspension baths consisting of 5% GelMA milled for 60s to which Matrigel and fibronectin are added, are suitable for bioprinting the Lund human mesencephalic (LUHMES) neural cell line, resulting in high cell viability and neuronal differentiation. We can conclude that suspended extrusion-based bioprinting of LUHMES cells in a soft suspension bath of GelMA microparticles reinforced with Matrigel and fibronectin, followed by neuronal differentiation, results in 3D growth of neurites that may form a neural network. These promising results support an easily accessible and widely applicable approach to bioprinting soft constructs, which can be employed to develop more advanced *in vitro* models including for PD, for disease modeling, drug-screening and drug-discovery.

Layman's Summary

Parkinson's disease is a common disorder that affects a rapidly increasing number of people worldwide. In Parkinson's disease, cells of the central nervous system stop working or even die, resulting tremors, stiffness, balancing issues, rigidity, and many other problems. The disease usually starts in adulthood and progresses over time, but no cure has been found yet. Therefore, it is important to study Parkinson's to reveal the causes and effects of the disease. Traditionally, we do this in simplified 2D models, which do not properly mimic the 3D environment of cells in the brain, or in animal models, which do not consist of human cells, meaning they cannot properly replicate human diseases. Therefore, in this project, we tried to print a small 3D piece of human brain tissue, as a more life-like prototype version of a disease model that we can use to study Parkinson's in the future. 3D bioprinting is a relatively new method in medicine to develop human tissue by extruding inks consisting of living cells, called bioinks, in a desired architecture. After the cells are printed, they can proliferate, specialize and mature to form a wide variety of tissues, including bone and cartilage. This tissue can be used for implantation into the body after injury or disease or it can be used in the lab to study disease mechanisms, as in our case.

First, we developed and characterized a support bath consisting of modified gelatin into which a bioink could be printed to prevent the collapse of the printed construct and to keep the cells of the construct in the right place. Since the brain consists of a high number of neurons in a relatively fluid environment, we replicated this by using soft, water-rich materials. Then, we printed with three different bioinks, consisting of cells and additional material to encapsulate the cells for protection and to make the ink flow smoothly out of the cartridge. Because cells generally do not like the printing process and easily get stressed or harmed, sturdy cells from the connective tissue were used to set-up and improve the printing process in the first part of the project. When that was established, embryonic stem cells were used in the second part of the project. They functioned as a precursor for the desired cells making up the construct in the third and last part of the project: neural cells. In this part, we added additional materials to the support bath and bioink to which the cells could bind to stimulate the formation of extensions of their cell body. These extensions are nerve fibers, which are essential for communication between neurons and the establishment of a well-functioning network that allows our central nervous system to perform actions.

In this project, we showed that the newly developed support bath was suitable for 3D printing of all three cell types and that they survived the printing process well. We can conclude that neural cells bioprinted into the support bath that was reinforced with additional materials, were able to specialize and become neurons. They formed many nerve fibers extending out to each other in multiple directions to form a 3D network. These promising results support a new strategy for printing soft constructs, which may help researchers worldwide to improve disease models, including those for Parkinson's. These may be applied in research, for drug-testing, and personalized medicine in the future.

1. Introduction

Parkinson's disease (PD) is a common, incurable neurodegenerative disorder that affects over 10 million people worldwide (Ou et al. 2021). Patients suffer from symptoms varying from tremors to stiffness, balancing issues, rigidity, a change in speech and many other problems. The disease mostly starts in adulthood and progresses over time. Most often, the cause of PD is unknown (idiopathic), but in some cases it is caused by a genetic defect, including mutations of the PARKIN, LRRK2, or α-synuclein gene. One of the key hallmarks of PD is the degeneration of dopaminergic (DA) neurons in the central nervous system (CNS), which is likely to be due to the aggregation of α-synuclein in Lewy bodies (Lew 2007; Henchcliffe and Flint Beal 2008; Jankovic 2008). In healthy individuals, these DA neurons project from the substantia nigra pars compacta to the striatum, where they release dopamine. The dopamine secreted in the striatum plays a major role in controlling movement, cognition, learning and mood, which explains the symptoms that people with PD suffer from. Astrocytes, the most abundant cell type found in the CNS, can also play a role in PD progression when they are malfunctioning, and some research also suggests that neuroinflammation contributes to PD (Lew 2007; Henchcliffe and Flint Beal 2008; Jankovic 2008). With the population aging, the number of PD patients is rapidly increasing (Ray Dorsey et al. 2018). Therefore, there is an emerging need to study PD.

The complexity of the brain poses a great challenge when studying brain disorders. It is a tissue that consists of 86 billion neurons, including DA neurons, and 85 billion non-neuronal cells, such as astrocytes and microglia, which are located in several different brain regions (Azevedo et al. 2009; Herculano-Houzel 2009). Because the brain is protected by the skull, it is particularly hard to study live affected tissue during disease. Therefore, most PD research is conducted post-mortem, in 2D *in vitro* cultures or *in vivo* using animal models. However, these models either lack the three-dimensional (3D) cell-cell interactions and complexity of the native brain microenvironment or are not comprised of human cells (Benam et al. 2015). Although postmortem tissue currently most accurately reflects PD pathology, obtaining this tissue presents a major obstacle.

To better replicate the *in vivo* native brain environment, increasing evidence suggests to study human cells in 3D cultures (Benam et al. 2015). 3D models not only provide support to cells, but also permit omnidirectional growth and migration of neurons, which is important for the formation of a neural network. Although it remains a great challenge to implement clinically relevant elements of a neurodegenerative disease in an *in vitro* model, one can start by recapitulating biologically quantifiable factors and phenotypes of PD in a model, such as the aggregation of α-synuclein and the loss of DA neurons (Lew 2007; Henchcliffe and Flint Beal 2008; Jankovic 2008).

For this purpose, biofabrication can be employed, which enables the precise deposition and patterning of biomaterials and cells to create more complex *in vitro* models. Unlike cerebral organoids (Lancaster et al. 2013) or 3D aggregates of neural cells (Smirnova et al. 2016), biofabrication aims to reconstruct functionality by designing constructs that reflect the architecture of brain-like tissue. The most commonly used biofabrication technique to print cells today is called extrusion-based bioprinting, in which a bioink is extruded to build a construct in a layer-by-layer fashion (Malda et al. 2013). The bioprinted construct can then be cultured over time and used for *in vitro* disease modelling, for drug-screening or for drug-discovery.

The aim of this study was to provide an answer to the following research question: can we establish a 3D *in vitro* neural network to study Parkinson's disease by suspended extrusion-based bioprinting of a cell-laden bioink? In order to reach this goal, the project was divided into the three following objectives: i) developing a suitable suspension bath to print a viable construct (designed to study PD) using human immortalized mesenchymal stromal cells (hiMSCs) to optimize the printing process ii)

developing a viable construct using human embryonic stem cells (hESCs), which can be differentiated into neurons induced by a growth factor protocol or viral transfection and which closely resemble induced pluripotent stem cells (iPSCs) in pluripotency, morphology, and behavior (Benam et al. 2015), which paves the way for developing a patient-specific PD model in the future, and iii) developing a viable construct of cells differentiated into neurons connected in a 3D neural network.

In the process of designing a construct that should replicate a brain-like structure, there are many properties to consider replicating. Two of these are the low stiffness, which lies around 1-13.6 kPa as described in the literature (Taylor and Miller 2004; Engler et al. 2006; Green et al. 2008; Kruse et al. 2008), and the high cell density of approximately 100M cells/ml of the brain (Braitenberg 2001; Cullen et al. 2006). These properties pose a challenge for the biofabrication process to develop novel strategies, since materials with a high viscosity and low cell density are easier to print (Malda et al. 2013).

In order to create a construct of low stiffness and high cell density, a protocol inspired by the freeform reversible embedding of suspended hydrogels (FRESH) technique described by Hinton in 2015 was established (Hinton et al. 2015). Hinton's method allows extrusion of a hydrogel of low mechanical stiffness into a secondary hydrogel support bath that keeps the extruded hydrogel in place in its intended 3D geometry and prevents it from collapsing. For their research, Hinton and colleagues use a suspension bath consisting of a slurry of gelatin microparticles that are obtained by milling a solid body of gelatin with phosphate-buffered saline (PBS) in a kitchen blender for a defined period of time. By blending a thermally gelated gelatin solution to create a slurry, the material obtains a self-healing, shear-thinning property that is highly valuable as a suspension bath. It acts as a Bingham plastic: it only flows after a threshold yield stress has been surpassed and it is rigid at low stress. Therefore, when the needle of the bioprinter runs through the slurry, the gelatin particles in front of the needle are liquefied, and those behind it gelate again by physical crosslinking to recover their formal solidity, which is necessary for continued support of the construct (Hinton et al. 2015; Cooke and Rosenzweig 2021). The success of the suspension bath is determined by its high self-healing yield stress, so that the printing needle does not affect the printability, its low thixotropy, and the quick recovery to its initial shape and viscosity after deformation (McCormack et al. 2020; Cooke and Rosenzweig 2021). FRESH allows printing of soft hydrogels, with an elastic modulus of <100 kPa that are usually challenging to print due to stability concerns (Hinton et al. 2015). Since gelatin is a thermosensitive hydrogel that liquefies at 35 °C, the gelatin dissolves and releases the 3D object when culture medium is added after printing (Hinton et al. 2015; Compaan et al. 2019). In recent years, many new formulations of suspension baths have been developed, including those consisting of agarose or Carbopol (Prendergast and Burdick 2021).

For this project, it was desirable to retain the suspension bath, in order to encapsulate the cells in the desired 3D geometry to maintain the high cell density of the neural construct. Therefore, instead of using a thermoreversible biomaterial such as gelatin, a crosslinkable material was selected: gelatin methacryloyl (GelMA), which is a biocompatible and highly tunable, photo-responsive gelatin derivative that closely resembles the gelatin used in the protocol established by Hinton (Hinton et al. 2015). The methacryloyl groups that have been added in GelMA allow for increased control over the gel's properties, such as the ability to covalently photocure the material by ultraviolet light in the presence of a photoinitiator (Yue et al. 2015; Compaan et al. 2019). Many properties of GelMA, including its mechanical properties, pore size, and degradation rates, can be easily tailored to its intended application (Schuurman et al. 2013; Yue et al. 2015). Because GelMA contains Arg-Gly-Asp (RGD) and GFOGER motifs (Knight et al. 2000), cells can bind to the hydrogel with their integrins and spread spatially in 3D, as opposed to merely horizontally in 2D cultures. Using gelatin-based support baths facilitates the fusion of mammalian cells and the formation of intercellular contacts within hours post-printing (Compaan et al. 2019).

Although the field of biofabrication has made great advances recently, the availability of functional bioinks is still a limiting factor. Whereas bioinks should be viscous enough to enable shape fidelity, this may limit cell viability. Bioinks of low viscosity, on the other hand, demonstrate low 'printability' as they have a tendency to flow and thus not retain their printed shape (Malda et al. 2013; Cooke and Rosenzweig 2021). To ascertain that the printed construct retains its shape after printing, coined its shape-fidelity, cell and tissue compatibility are often compromised. Novel hydrogels aim to maintain shape-fidelity despite a low stiffness and polymer concentration (Malda et al. 2013). Printability and shape-fidelity are important parameters that were also taken into account during this project, because of the low mechanical stiffness of brain tissue. The materials used should therefore be rather fluid, but still viscous enough for the printing process.

This research report will first present an extensive characterization of a newly formulated, crosslinkable milled GelMA suspension bath. Then, the application of this bath to enable printing of a bioink of low mechanical stiffness will be described in detail for three different cell types: for hiMSCs, for hESCs, and for the Lund human mesencephalic (LUHMES) neural cell line. This will include an evaluation of the influence of several printing parameters, including printing pressure and feedrate, on the shape fidelity, filament width, and cell viability of the extrusion-bioprinted construct. To our knowledge, in this paper, we demonstrate the first attempt to print a neural cell-laden bioink in a milled GelMA suspension bath to establish a 3D neural network that aims to allow cell-cell interactions that are characteristic for the substantia nigra of the brain.

2. Materials and Methods

2.1 Preparation and analysis of milled GelMA suspension baths

2.1.1 Preparation of milled GelMA suspension bath

To make milled GelMA suspension baths, 5% (w/v) sterile, lyophilized, porcine GelMA (synthesized on 08/08/2021, 85% degree of functionalization (DoF) as determined by trinitrobenzenesulfonic (TNBS) acid analysis, batch 23) was weighed and dissolved in PBS by incubation at 37°C for at least 20 mins. It was then gelated at 4 °C overnight. A 500 ml Oster® blender mason jar was cleaned with Biocidal ZF™ and 70% ethanol, sterilized by UV for at least 20 mins, and also stored at 4 °C overnight. The next day, cold PBS was added to the jar to make up a total volume of 100 ml with the solid block of gelated GelMA. The GelMA was milled at "pulse" speed and the contents of the jar were centrifuged at 4000 rpm for 4 mins at 4°C to separate the GelMA microparticles from the PBS. After centrifugation, the supernatant was aspirated and, in case bubbles were present, the milled GelMA was washed with cold PBS and centrifuged again until all bubbles were removed. The GelMA slurry was be stored at 4 °C until further use. In order to crosslink the GelMA, powdered Lithium Phenyl-2,4,6-trimethylbenzoylphosphinate (LAP)(Tokyo Chemical Industry CO. Ltd., L0290) was dissolved in PBS to reach a working concentration of 2% (w/v), which was sterilized using a 0.22 µm filter.

2.1.2 Microparticle size

To measure the effect of the blending time on GelMA microparticle size, the procedure described in 2.1.1 was followed to obtain milled GelMA. The GelMA was blended at "pulse speed" for 45s, 60s, 90s, and 120s and centrifuged at 4000 rpm for 4 mins at 4°C. For each blending time, 200 µl of milled GelMA was placed on a cover slide on ice, stained with 10 µl food dye, and diluted with 200 µl PBS. Microparticles were imaged with the Olympus SZ61 microscope. For each condition, the diameter of 350 particles was measured and analyzed using ImageJ (National Institute of Health)(Supplementary Fig. S1). To analyze the data, an ordinary one-way ANOVA was conducted in GraphPad Prism. Different groups represented different blending times and a Gaussian distribution of residuals was assumed. For multiple comparisons, the mean of each column was compared with the mean of every other column and the results were corrected for this using Bonferroni statistical hypothesis testing.

2.1.3 Mechanical Testing

To measure the effect of the GelMA concentration (w/v) and blending time on the stiffness of bulk and milled GelMA respectively, a series of samples were prepared for dynamic mechanical testing (DMA). For samples consisting of milled GelMA, GelMA was blended for 45s, 60s, 90s, and 120s and LAP was added to 500 µl of the cold, already milled GelMA (4°C) to obtain a final concentration of 0.1% (w/v). The milled GelMA was then pipetted into a 3D printed Teflon mold to create three GelMA discs with a height of 2 mm and diameter of 6 mm per blending time (n=3). For samples consisting of bulk GelMA, 3%, 4%, and 5% bulk GelMA were prepared and LAP was added to 500 µl the warm GelMA (37°C) to obtain a final concentration of 0.1%. It was then pipetted into a 3D printed Teflon mold to create three GelMA discs with a height of 2 mm and diameter of 6mm per concentration (n=3). The molds were placed in the fridge until they were 4°C, to allow for proper comparison with the milled GelMA discs. All samples were crosslinked for 5 mins at 365 nm with a UV light lamp (Vilber Lourmat UV Lamp, Collegien, France) at room temperature and incubated at 37°C in PBS overnight to replicate the temperature of the samples during cell culture.

The mechanical properties of all samples were assessed the following day in accordance with stress-relaxation and compression protocols (Appendix) to determine the Elasticity and Young's modulus

respectively. In between measures, the samples were kept at 37°C to maintain the same conditions for each sample. To determine the Elasticity of the material (in %), the highest strain was divided by the strain at the time of relaxation (2 mins). To determine the stiffness of the material, the stress was plotted against the strain and the slope of the linear part of the graph (from x=0.1 until x=0.15) was calculated.

$elasticity = \frac{highest\ strain}{strain\ at\ 2\ mins} * 100$ $stress\ (\sigma) = \frac{F\ (N)}{A}$ $strain\ (\varepsilon) = \frac{-\Delta h}{h}$

F: static force in Newton, A: area of the sample in mm^2 ($A = \pi r^2$), Δh: displacement in µm and h: height of the sample in µm.

2.1.4 Swelling Ratio and Sol Fraction

To assess the effect of blending on the swelling ratio and loss of uncrosslinked macromeres of the GelMA after crosslinking, a sol fraction analysis with two conditions was performed. For each sample, 500 µl of 5% bulk GelMA and 5% GelMA blended for 60s with 0.1% LAP was pipetted into a well of a 48 wells plate (as in the final experiment with LUHMES cells) and crosslinked for 5 mins at 365 nm (n=3). Samples were frozen for 30 mins and lyophilized overnight. The next day, the initial dry mass of the samples was weighed ($m_{dry,t0}$), after which the samples were soaked in PBS and incubated at 37 °C overnight. On the third day, the weight of the swollen samples was recorded ($m_{swollen,t1}$) and the samples were frozen and lyophilized overnight again. On the last day, the dry weight of the samples was measured again ($m_{dry,t1}$). The mass swelling ration and sol fraction or percentage of mass loss of uncrosslinked macromeres in the hydrogel network can be calculated with the following formulas: mass swelling ration (q): $q = \frac{mswollen,t1}{mdry,t1}$ and $sol\ fraction = \frac{mdry,t0 - mdry,t1}{mdry,t0} * 100\%$.

2.2 Cell culture

In this project, hiMSCs, hESCs, and LUHMES were cultured in a 95% humidified incubator at 37°C, 5% CO_2. Per cell type, specific culturing methods (below) and media (Appendix) were used.

2.2.1. hiMSCs

hiMSCs were expanded in alpha Modified Eagle Medium culture medium (α-MEM, Gibco™, Life Technologies) supplemented with 10% fetal bovine serum (FBS), 1% Penicillin Streptomycin (Penstrep), 1% L-ascorbic acid-2-phosphate (AsAP) and 1 ng/ml basic fibroblast growth factor (bFGF). They were plated at 0.4M cells/T175 culture flask, medium was changed twice a week and hiMSCs were passaged every 5-7 days depending on confluency, by detaching with trypsin for 2 mins at 37°C. The detached cultures were resuspended to single cells and plated in new T175 culture flasks. To obtain a cell pellet, cells were centrifuged at 1500 rpm for 4 mins.

2.2.2. hESC

Undifferentiated, pluripotent hESCs (H1 cells) were cultured in Stemflex™ medium. After 5 days of culturing or after reaching over 70% confluency, hESCs were plated at a 1:10 ratio. Stemflex™ medium was changed every other day, and cells were passaged every 4-5 days by detaching with 500 µl ReleSR that was aspirated again and incubated for 2 mins at 37°C. The detached colonies were resuspended several times to obtain small clumps of cells to be passaged to 6-well plates. Prior to passaging, wells were coated with Corning® Matrigel® hESC-Qualified Matrix (LDEV-free, product number 354277, qualified for use with mTeSR™ and medium by StemCell Technologies)(Slater et al. 2018). Matrigel was thawed at 4°C on ice overnight and dissolved in cold medium (DMEM/F12) to reach a concentration of 11,2 µl Matrigel/ml (for the batch that was used during this project). Subsequently, 1 ml of Matrigel solution was added to each well and left to coat the well at room temperature for 45 mins. Then, Matrigel was aspirated, 1 ml of Stemflex was added to each well and cells were passaged.

2.2.3. LUHMES

LUHMES were expanded in neural expansion medium. For neural differentiation, a protocol adapted from Scholz (Scholz et al. 2011) was used prior to and post-printing. For this purpose, neural differentiation medium was used (Appendix), which contains the antibiotic doxycycline (dox) to inhibit gene expression via the tet-off system, a genetic manipulation technique that is used to spatially and temporally control gene expression (Scholz et al. 2011). Other supplements included dibutyryl-cyclic-AMP (db-cAMP) to stimulate neurite outgrowth, neural differentiation and maturation (Imamura and Ozawa 1998; Scholz et al. 2011; Knott et al. 2014) and glial cell- and brain-derived neurotrophic factors (GDNF and BDNF) to promote survival of and induce differentiation to DA neurons . Culturing LUHMES in 3D affects their differentiation as it results in the alteration of exogenous factors such as the availability of nutrients, cell attachment, and cell-cell interaction (Scholz et al. 2011; Smirnova et al. 2016; Harris et al. 2017).

After 2 days of differentiation in 2D monolayer conditions, LUHMES cells were harvested from culture flasks by detaching with 3 ml trypsin+EDTA for 7 mins at 37°C. Additional care was taken when passaging LUHMES cells, because of their tendency to stick to each other and culture plastics. Cells were centrifuged at 200G for 2 mins to obtain cell pellets that were resuspended in biomaterial to make up the bioink. In parallel to 3D experiments, 2D differentiation studies with LUHMES were conducted to confirm that the differentiation protocol indeed resulted in LUHMES proliferating and forming neurites.

2.3 3D bioprinting process

In this project, the RegenHU 3D Discovery was used to print 3D constructs, using a 3ml cartridge and a conical, plastic, 25 Gauge (25G) nozzle with an inner diameter of 260 µm and outer diameter of 514,4 µm (Precision Tips, Engineered Fluid Dispensing, Nordson EFD). Before printing, the cartridge and piston were autoclaved and the nozzle, endcap, and cap were immersed in 70% ethanol for 5 mins and UV'ed for at least 20 mins (all printing tools from Nordson EFD). Wells of either a 24 or 48 wells plate were filled on ice with respectively 750 µl or 500 µl suspension bath material. The plates were covered with aluminum foil to prevent crosslinking due to UV exposure and stored at 4°C until the start of the printing process.

Cells were detached as described in 2.2, counted, filtered with a 100 µm cell strainer to remove cell strands and well coating residues if necessary, and centrifuged to obtain cell pellets that could be resuspended in the appropriate biomaterial to form a bioink as described below. In every experiment, before the cartridge was loaded, the bioink was manually pipetted into a control well, to evaluate the effect of the printing process on the cell viability. Then, the bioink was carefully pipetted into the cartridge, which was closed off at the bottom with the end cap. The piston was then placed on top of the cartridge and pushed in slightly. The cartridge was turned around and the piston was pushed further into the cartridge until the bioink was compacted at the top of the extrusion-side of the cartridge and could be sterilely closed off with the end cap and cap.

To commence the printing process, the end cap of the loaded cartridge was replaced by the nozzle, the cap was removed to attach the pressure valve and the cartridge was placed into the printhead and secured tightly. The printing pressure was set and the printhead holding the cartridge with nozzle attached was calibrated to print in the middle plane of the GelMA suspension bath. The set-up of the printing process is depicted in Supplementary Fig. S2. Constructs in the shape of a serpent, as depicted in Fig. 1, which were coded by the manually written G-code (Appendix), were then bioprinted. Due to limited plastics supply caused by the COVID-19 pandemic, 24 wells plates from several different manufacturers were used (Sarstedt, Corning), requiring the design of different G-codes as dictated by the well plates' varying dimensions. In the Appendix, only one G-code per 24

and 48 wells plate is shown, because of a large amount of overlap except for specific coordinates. After printing, the constructs were crosslinked for 5 mins at 365 nm UV light. Subsequently, medium was added to each printed sample for cell culture.

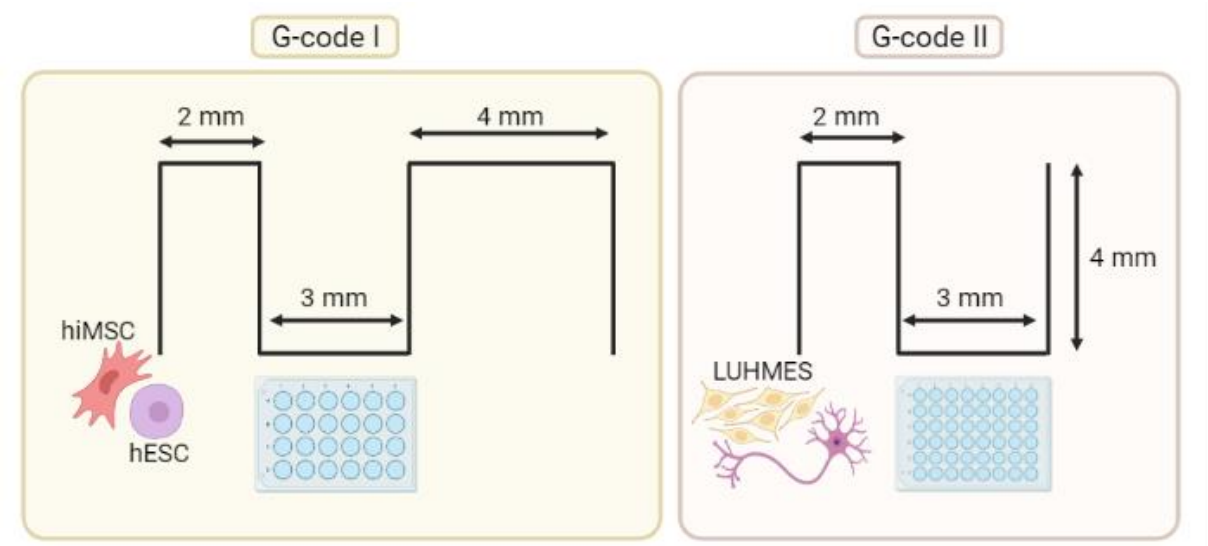

Fig. 1. Schematic of the construct shape to be printed with the RegenHU 3D Discovery in 24 (left) and 48 (right) wells plates. The black print path shows the geometry of the bioink that is to be extruded.

2.3.1 Printing hiMSC

For printing hiMSCs, powdered gelatin (from bovine skin, G9391, 225 bloom, Sigma Aldrich) was dissolved in PBS in a hot water bath at 60°C for 20 mins to reach a final concentration of 5% (w/v). Directly after, the warm gelatin was sterilized using a 0.22 µm filter and 0.1% LAP was added. The cell pellet of hiMSCs was resuspended in gelatin to form the bioink. hiMSCs were printed in the 5% gelatin bioink at a cell density of 50M cells/ml, in a 24-wells plate filled with a 5% GelMA suspension bath milled for 60s with 0.1% LAP.

2.3.2 Printing hESC

For printing hESCs prior to differentiation into dopaminergic neurons, cells were cultured following the aforementioned protocol, but detached with 1ml Accutase for 7 mins at 37°C to obtain single cells instead of colonies, to allow viral transfection after printing. To obtain a cell pellet, cells were centrifuged at 300 rpm for 5 mins and resuspended in the appropriate biomaterial to form a bioink. For hESCs, powdered gelatin (from bovine skin, G9391, 225 bloom, Sigma Aldrich) was dissolved in PBS in a hot water bath at 60°C for 20 mins to reach a final concentration of 5% (w/v). Directly after, the warm gelatin was sterilized using a 0.22 µm filter, 0.1% LAP was added, and the cell pellet of hESC was resuspended in the gelatin to form the bioink. hESCs were printed in the 5% gelatin bioink at a cell density of 50M cells/ml, in a 24-wells plate filled with a 5% GelMA suspension bath milled for 60s with 0.1% LAP.

2.3.3 Printing LUHMES

To assess if the printing parameters and conditions suitable for printing hiMSCs and hESCs were also appropriate for printing LUHMES, a preliminary print with LUHMES cells was performed (Fig. 2). First, a 5% GelMA suspension bath milled for 60s was prepared and wells of a 24 wells plate were filled. Then, a 5% gelatin bioink was prepared and harvested LUHMES were resuspended at a cell density of 25M cells/ml. The cartridge was loaded and gelated in a water bath at 25 °C for 35 mins and subsequently samples were printed. After printing and crosslinking, differentiation medium was added to each printed sample for cell culture. Medium was changed every 2 days. A schematic

overview of the experiment can be found in Supplementary Fig. S3. Samples were imaged at t1, t3, t4, and t5 using the Leica DMi1 inverted microscope.

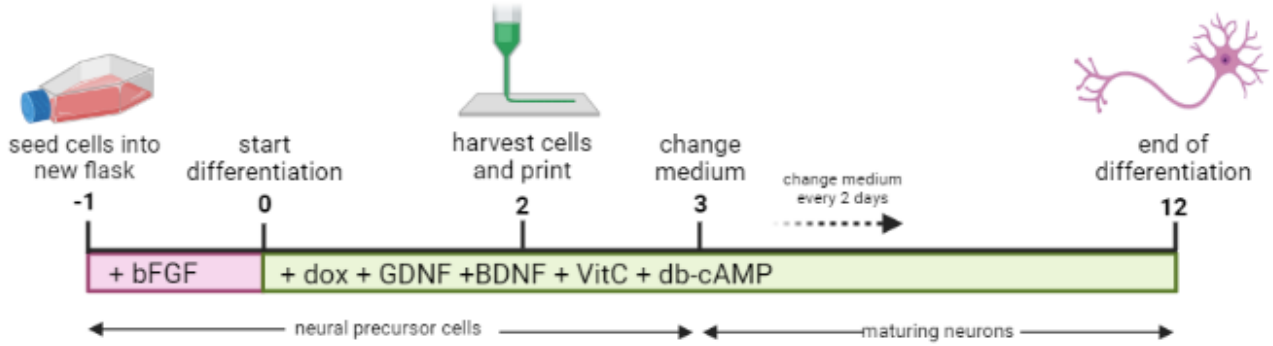

Fig. 2. LUHMES printing and differentiation protocol prior to and post-printing.

For the final experiment, 5% GelMA was milled for 60s to which LAP (0.1%), Matrigel (11,2 µl/ml) and fibronectin (50 µl/ml)(fibronectin bovine plasma, Sigma Aldrich, F1141-1MG) were added. First, wells of a 48 wells plate were filled with 500 µl of the reinforced, milled GelMA, kept cold on ice, covered with aluminum foil to prevent crosslinking due to UV exposure and stored at 4°C until the start of the printing process. Differentiation medium was prepared prior to printing, so that it could be added to the samples directly after crosslinking.

Next, LUHMES cells were harvested and centrifuged and pellets of LUHMES cells were resuspended in 3 ml of the reinforced, milled GelMA to obtain a bioink at a cell density of 10M cells/ml. This bioink was first manually pipetted into the control wells and then loaded into the cartridge with a gel pipet. The bioink was printed into the GelMA suspension baths at a printing pressure of 13 kPa and crosslinked. Then, 300 µl differentiation medium was added to each sample. In total, 28 samples were printed, of which 4 per feedrate (F3-F6) and 2 pipetted controls. One 24 wells plate was seeded as a 2D control.

2.4 Cell Viability Assays to determine Printing Resolution and Filament Width

To assess cell viability after the printing process on day 1 and day 7, live/dead assays were performed. Cells in printed samples were stained with Calcein-AM (Invitrogen™, C1430, 2ug/ml), which yields a green cytoplasmic fluorescence after being cleaved by esterases in live cells, and Ethidium Homodimer-1 (EthD-1, Invitrogen™, 1 µg/ml), whose fluorescence is a measure of membrane permeability and cell death to indicate dead cells. The samples were washed with PBS+ twice for 5 mins before a dilution of the two dyes in PBS+ was added. The plate was then covered with aluminum foil and incubated for 30 mins. Before fluorescence imaging, the samples were washed twice for 5 mins with PBS+. Samples were imaged directly after using the Thunder or Confocal microscope (Leica) and Leica Application Suite X imaging software and further analyzed using ImageJ. Cell viability was quantified after splitting the red and green channels and counting cells by point selection, after which the cell viability was calculated with the following formula: $percentage\ of\ live\ cells = \frac{live\ cells}{live\ cells + dead\ cells} * 100$ (Supplementary Fig. S4).

To analyze the effect of printing pressure and feedrate on the printing resolution of hiMSCs and hESCs, the diameter of the filament was measured five times per straight filament of the serpent-shape, for a total of 35 measurements per sample for three samples per condition (n=3) for hiMSCs and two samples per condition (n=2) for hESCs.

To analyze the data of the hiMSC prints, an ordinary Two-Way ANOVA was conducted in GraphPad Prism. In the grouped table, one variable was Printing pressure (kPa) and the other Feedrate (mm/s). Cell means were compared regardless of rows and columns. The results were corrected for multiple comparisons using Bonferroni post-hoc statistical hypothesis testing. To analyze the data of the hESC prints, a one-way ANOVA was conducted in GraphPad Prism. A Gaussian distribution was assumed. In the grouped table, the variable was Feedrate (mm/s). Cell means were compared and the results were corrected for multiple comparisons using Bonferroni post-hoc statistical hypothesis testing.

To assess cell viability of LUHMES cells after the printing process of the final print, on day 1 and day 7, live/dead assays were performed following the protocol described above. Cell viability was calculated for 2 of the 4 prints per feedrate (F3-F6) and both manually pipetted controls. Of each sample, 3 random sections were imaged and cells were manually counted using ImageJ.

2.5 Neuronal Differentiation Studies using Immunocytochemistry

For immunostaining, samples were fixed and stained to visualize βIII-tubulin, TH, and nuclei, using an immunocytochemistry protocol for staining cells in 2D that was altered for staining 3D samples. In order to do so, medium was removed and 3D samples were washed carefully three times with PBS before 4% paraformaldehyde (PFA) was added to fixate the cells at room temperature for 10-15 mins. Then, samples were washed with PBS again. After this step, PBS with sodium azide (NaN_3, 0.02%) could be added to preserve the samples until staining while preventing contamination. For permeabilization of the cell membrane, 0.1% Triton-100 was incubated at room temperature for 15 mins, after which the samples were washed with PBS again. To prevent non-specific binding of antibodies to membrane proteins instead of the target protein, 3% Bovine Serum Albumin (BSA, Sigma) blocking solution was then added and incubated at room temperature for 1.5 hrs for 2D samples and 3 hrs for 3D samples. After this step, primary antibodies diluted in BSA were added and incubated overnight at 4°C for 2D samples and at room temperature for 3D samples. To stain TH, a primary rabbit antibody (1:500) was used, and to stain βIII-tubulin, a primary mouse antibody (1:500) was used. After the incubation period, the samples were washed at low rocker speed with PBS 3 times for 5 mins for 2D samples and 2 times 5 hrs for 3D samples. Next, secondary antibodies diluted in BSA were added to the samples and incubated in the dark at room temperature for 1.5 hrs for 2D samples and overnight for 3D samples, using goat antimouse IgG AlexaFluor™ 488 (Invitrogen; 2mg/ml) and goat antirabbit IgG AlexaFluor™ 555 (Invitrogen; 2mg/ml). Following this step, the nuclei were stained at room temperature for 15 mins with 4',6-diamidino-2-phenylindole (DAPI)(Sigma Aldrich, D9542, 1:500, 1 mg/ml) to yield a blue nucleic fluorescence by binding to nucleic acids. Finally, samples were washed with PBS and covered with aluminum foil until imaging. For 3D samples, washing steps following incubation with antibodies were increased from 3x5 mins to 3x2 hrs. Samples were imaged with the Thunder microscope and Leica Application Suite X imaging software and further analyzed using ImageJ.

Two preliminary experiments to find out the best conditions for neurons to form neurites suspended in milled GelMA were conducted.

2.5.1 LUHMES suspension - biomaterials

For the first experiment, cell pellets of LUHMES cells were resuspended to reach a cell density of 20M cells/ml in four different 5% GelMA milled for 60s conditions to assess whether the LUHMES cells would stay alive, form aggregates and/or form neurites when resuspended in this particle reinforced 3D milled GelMA microenvironment. The four conditions consisted of milled GelMA only, milled GelMA with Matrigel, milled GelMA with fibronectin, and milled GelMA with Matrigel and fibronectin (n=2). For Matrigel, the concentration normally used to coat wells was used (11,2 µl/ml) and for fibronectin the concentration that is used for bioinks (50 µl/ml) was used. Differentiation medium was prepared before making the cell suspensions, so that it could be added to the samples directly

after crosslinking. A 96 wells plate was used to reduce the volume required to make the 8 samples, considering the small cell size of the LUHMES. Samples were imaged at t0, and t4, using the Leica DMi1 inverted microscope.

2.5.2 LUHMES suspension - cell densities

The second experiment was performed to assess the most suitable cell density for the bioink to form neurites. For this purpose, cell pellets of four different LUHMES cell counts were resuspended in milled GelMA with Matrigel (11,2 µl/ml) and fibronectin (50 µl/ml): 10M cells/ml, 15M cells/ml, 20M cells/ml, and 25M cells/ml. Differentiation medium was prepared before the experiment to be added directly after crosslinking. A 96 wells plate was used again to reduce the volume required to make 8 samples. To demonstrate proof of neuronal differentiation and dopaminergic maturation, samples were fixed at t8 and t12, and stained to detect the presence of neuronal marker βIII-tubulin, dopaminergic marker TH, and DAPI, using an updated staining protocol for 3D samples, that was adjusted by incubating the primary and secondary antibody for 48 hrs at room temperature instead of overnight, incubating DAPI for 3 hrs instead of 15 mins, and increasing the number of washing steps to 3x2 hrs instead of 2x5 hrs. After staining, samples were scooped out of their well, transferred onto a glass slide and imaged by Confocal microscopy using Leica Application Suite X imaging software.

2.5.3 LUHMES print

In order to demonstrate proof of neuronal differentiation and dopaminergic maturation of the final LUHMES print, printed samples were fixed on day 8 after printing (day 10 of differentiation). The immunocytochemistry staining protocol for 3D samples was slightly altered again by reducing the incubation time of DAPI from 3 hrs to 1 hrs. Samples were scooped out of their well, transferred onto a glass slide and imaged by Confocal microscopy using Leica Application Suite X imaging software.

2.6 Statistics

The results shown in this report are means ± standard deviations. For statistical analysis, multiple comparisons were conducted with an unpaired student's t-test, one-way analysis of variance (ANOVA) or two-way ANOVA with a Bonferroni's post-hoc test as appropriate, using GraphPad Prism 8 (GraphPad Software, USA) statistics software, where values of $p<0.05$ (95% confidence level) were considered significant.

3. Results and Discussion

3.1 Preparation and characterization of milled GelMA suspension bath

Here, we report the development and characterization of a highly tunable and crosslinkable GelMA-based suspension bath that allows FRESH-inspired 3D bioprinting to create a cell dense neural construct. In their review, Yue *et al*. discuss the use of GelMA in a broad variety of microfabrication techniques to create GelMA hydrogel constructs, such as photopatterning, stacking of layers, micromolding, self-assembling, microfluids, bioprinting, and biotextile (Yue et al. 2015). To the author's knowledge, this is the first report of the development and characterization of a milled GelMA suspension bath, as an addition to the already existing range of suspension bath formulations to further expand the application of extrusion bioprinting of constructs of low mechanical stiffness.

3.1.1 Preparation of milled GelMA suspension bath

For this project, sterile, lyophilized, porcine GelMA that was synthesized for general use by our group was used. The DoF was determined by TNBS acid analysis at 85%. Because GelMA is a natural hydrogel derived from an animal source, batch-to-batch variation presents a considerable challenge when working with this biomaterial. Therefore, for all of the results presented in this research report the same batch of GelMA was used. To make the milled GelMA suspension baths, the protocol developed by Hinton and colleagues (Hinton et al. 2015) for preparing gelatin suspension baths was adjusted for use with GelMA, by experimental analysis and trial-and-error. This was a challenging and time-consuming process, because the GelMA often dissolved during blending. It was decided that the jar and GelMA should therefore be placed in the fridge overnight prior to blending, to keep the temperature low to prevent dissolution. Still, the GelMA often dissolved at higher concentrations, for example between 7-10%. This is probably due to the swelling ability of the GelMA, which attracts and soaks up more PBS at high concentrations (Aubin et al. 2010). Another adjustment to Hinton's protocol was filling the mason jar to make up a total volume of 100 ml instead of to the brim, as the latter results in having to use a superfluous amount of lab plastics and pipetting together small volumes of milled GelMA (a process in which a considerable amount of material is lost). When the volume in the jar is 100 ml, the blender blades are sufficiently submerged and the total blended volume can be nicely centrifuged in two conical 50 ml tubes. Lastly, it was found that when LAP was mixed with GelMA before blending, most LAP was aspirated with PBS after blending, which resulted in very limited crosslinking. Therefore, LAP should only be added after blending and resuspended with a gel pipet to ensure proper dispersion throughout the gel without the formation of air bubbles.

3.1.2 Milling for 60s results in the optimal microparticle slurry

In order to replicate the native brain microenvironment as closely as possible, while keeping the large amount of cells of the 3D bioprinted construct in place, a crosslinkable suspension bath with a low viscosity that is easy to handle over a long culture period is required. The most common way of adjusting the stiffness of GelMA is by changing the GelMA concentration. In order to stimulate cell extension and tissue development, gelatin and GelMA concentrations should be kept as low as possible, while maintaining the ability to preserve their supportive function (Compaan et al. 2019). Therefore, the optimal GelMA concentration was determined: one that is as low as possible to achieve a low mechanical stiffness, but one that is high enough to enable crosslinking and easy handling during experiments. For this purpose 5% GelMA seemed most suitable. Since GelMA is a polymer of natural origin, it has a limited capacity regarding printing resolution and shape fidelity, so it is important to characterize its properties as much as possible. Prendergast *et al.* have demonstrated that computational analysis of print speed and the interaction between suspension

bath and ink are a powerful tool, but cannot fully predict how a suspension bath will behave (Prendergast and Burdick 2021). Therefore, rheology and experimental testing are required.

In order to optimize the printing accuracy and resolution, it is favorable to use a suspension bath that consists of slurry with the smallest microparticle size that is still able to crosslink. Moreover, a homogeneous suspension bath is desirable, to limit the effect of microparticles of varying sizes affecting the resolution (Prendergast and Burdick 2021). By varying the blending time, the size of gelatin microparticles can be influenced (Hinton et al. 2015). This is important, since it influences printing resolution and cell viability: large particles not only result in bigger pores, through which nutrients can easily access the cells of the printed construct, but also in a bad resolution, whereas the opposite holds for small microparticles. Therefore, the effect of four different blending times on microparticle size was assessed: 45s, 60s, 90s, and 120s (Supplementary Fig. S5). It was hypothesized that microparticle size decreases with increasing blending time. Blending times above 120 s were not included, because in these conditions, the GelMA particles entirely dissolve in PBS during blending, resulting in 100 ml of diluted GelMA.

Based on the results of this experiment, we can conclude that milling 60s results in the optimal microparticle suspension bath. The histogram in Fig. 3A shows the Gaussian distributions of the microparticle size for different blending times. Here, it becomes apparent that GelMA slurries blended for over 45s are significantly more homogeneous, with the GelMA blended for 90s resulting in the most homogeneous slurry, closely followed by those blended for 60 and 120s. It can be seen that the microparticle size decreases with increasing blending time and that the standard deviation decreases significantly when blending for over 45s (Fig. 3B).

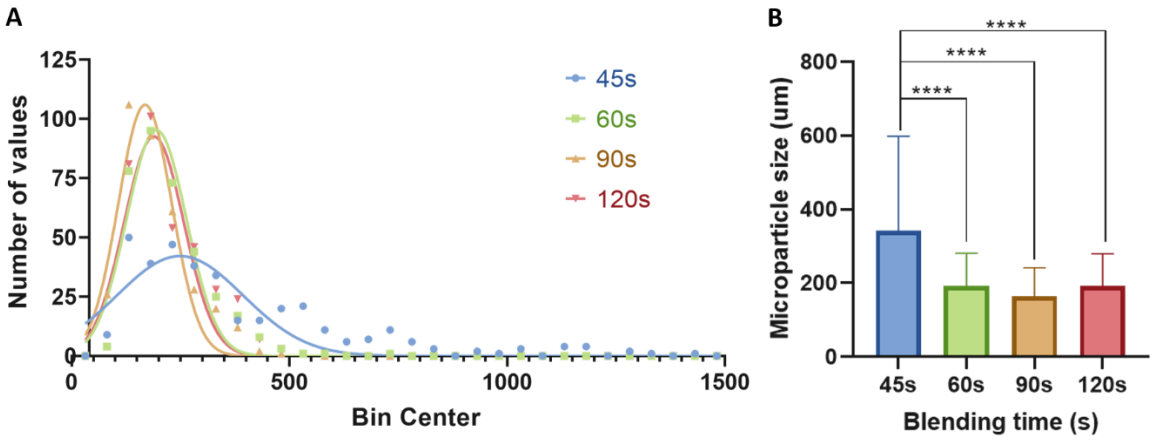

*Fig. 3. Characterization of microparticles. A) Gaussian distribution of GelMA microparticle size produced by different blending times. The mean of the bell shaped curve or Gaussian distribution (μ) is a value referring to the corresponding bin center and the standard deviation (σ) is determined by the width of the curve. (n=350 per blending time). B) Bar graph showing the mean size and SD of GelMA microparticles after various blending times (****$p \leq 0.0001$).*

Interestingly, in this experiment, particles obtained after 120s of blending are slightly larger than those blended for 60s and 90s, which is presumably due to the fact that particles of a smaller size are the less visible and thus harder to count, because the stain is less bright. Larger particles, on the other hand, can be more easily detected, resulting in an overestimation of particle size (especially for the 120s condition). The difference in microparticle size between the GelMA milled for 60s, 90s, and 120s is neglectable as it falls within the error of the experiment ($p>0.05$). Therefore, based on the results from this microparticle size assay, using GelMA milled for over 45s is the most suitable option for the development of our model, as it results in a homogenous slurry of small particle size.

A simple measurement of the pH of our suspension bath with pH test strips pointed out that 5% GelMA slurries blended for 45s, 60s, 90s, and 120s all had a pH of 6.5. This means that increasing the blending time is likely not to disturb the chemical bonds in the GelMA in such a fashion that it has a significant effect on the pH. Since medium surrounding the samples has the right pH, corresponding to the extracellular pH of eukaryotic cells, which is maintained at 7.3-7.4 during homeostasis (Casey et al. 2010), a pH of 6.5 is likely to be acceptable for the encapsulated cells.

3.1.3 Milling for 60s results in mechanical stiffness <20 kPa

Next, the Young's modulus and elasticity of a range of milled GelMA samples was determined. The mechanical properties of bulk GelMA samples were also assessed, to demonstrate the effect of milling on the Young's modulus and elasticity. Hydrogel stiffness is an important characteristic of both the biomaterial in the bioink and the suspension bath, as it influences their mechanical properties as well as the behavior and morphology of cells that are encapsulated by it (Li et al. 2016). The stiffness is determined by the degree of methacrylation, the DoF, the degree of crosslinking, the biomaterial concentration, as well as the temperature and, in case of slurries, blending time (Li et al. 2016).

It was found that the stiffness of samples consisting of bulk GelMA increased with increasing concentration (Fig. 4A) and that the stiffness of samples consisting of milled GelMA decreased with increasing blending time (Fig. 4B). Of note is the Young's modulus of 5% GelMA crosslinked at 4°C (Fig. 4A), which is high compared to GelMA crosslinked at 37°C (not depicted here). This is important to consider as the crosslink temperature apparently affects the stiffness of the final construct. Lastly, it was found that the elasticity of all samples was between 95% and 100% (Fig. 4C), meaning that in a crosslinked suspension bath, GelMA is likely to hold the printed cells in place to maintain the shape fidelity of the construct.

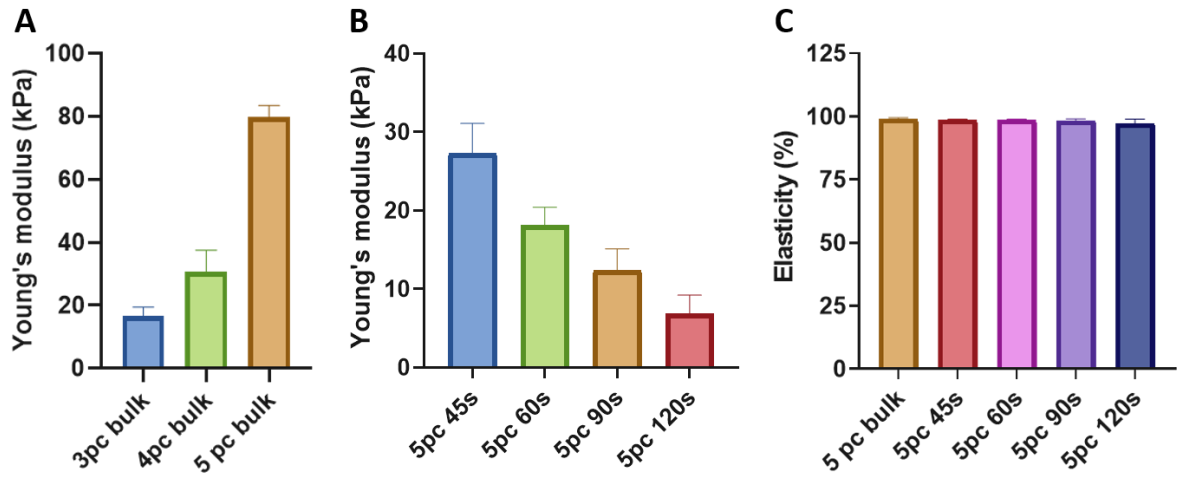

Fig. 4. Mechanical properties of bulk and milled GelMA. A) Young's modulus of bulk GelMA B) Young's modulus of milled GelMA C) the elasticity of bulk and milled GelMA samples. When calculating the Young's modulus, all R^2 values were greater than 0.97.

Based on the results from this experiment, milling 5% GelMA for 60s results in the most appropriate stiffness for the development of our model as obtainable by this methodology. The 60s milled GelMA has a Young's modulus of 18.1 ±2.3 kPa: the lowest stiffness that results in a gel that is still easy to handle and remains stable over time. Blending over 60s limits the resulting scaffold's ease of handling and therefore the shelf-life of the intended *in vitro* model. This is especially undesirable considering medium exchanges and washing steps required for immunocytochemistry for example. Moreover, it is also clear one should not use a bulk GelMA bioink for our application, since the bulk

GelMA stiffness is not only a lot higher than that of milled GelMA, meaning that the cells would not be able to migrate and proliferate easily in the printed construct whereas they would in the surrounding suspension bath, but also too high compared to the native brain environment. Bulk GelMA would not be applicable for use as a suspension bath, because it is not granular, meaning that the nozzle would cleave the suspension bath during printing. Instead, during the printing process, the milled GelMA suspension bath should act as a Bingham plastic: when the nozzle moves through the slurry it demonstrates shear-thinning properties, whereas it is highly viscous when no stress is applied (Cooke and Rosenzweig 2021). Because of the shear-thinning properties of the milled GelMA, bioink can be deposited in multiple planes, without the disruption of previously printed filaments.

It is important that the mechanical properties of the 3D model, including the hydrogel stiffness, replicate the native brain microenvironment as the elasticity of the matrix has a strong effect on cell structure, function, behavior (Flanagan et al. 2002; Shin et al. 2012) and even direct stem cell lineage specification (Engler et al. 2006). Culturing cells on a soft matrix with the stiffness of the brain, results in adhesion, spread, branching, filopodia formation and the expression of markers of neural commitment and maturity (Engler et al. 2006). Flanagan *et al.* have shown that neurons cultured on softer matrigel substrates form over three times as many neurite branches as those cultured on stiffer gels of the same material (Flanagan et al. 2002). Therefore, it is worth noting that the stiffness of our hydrogel is not optimal yet, but lies close to the range of native human brain tissue, which ranges between 1-13.6 kPa as described in the literature. These numbers vary depending on their methodology: most of these studies were conducted with samples in Matrigel, reflecting the lower end of the spectrum in terms of mechanical stiffness, whereas others were obtained by magnetic resonance elastography (Taylor and Miller 2004; Engler et al. 2006; Green et al. 2008; Kruse et al. 2008). Nevertheless, we can conclude that the mechanical stiffness of our hydrogel should still be slightly lowered.

3.1.4 Swelling Properties of 5% milled and bulk GelMA are comparable

In the following experiment, the swelling ratio of samples was compared between bulk GelMA and GelMA blended for 60s. The sol fraction and swelling ratio of a hydrogel are important characteristics to consider as they affect the final mechanical and physical properties of the construct, as well as the diffusion of nutrients and small molecules such as antibodies through its pores (Peppas et al. 2006; Malda et al. 2013). For this project, a minor swelling of the construct would not be detrimental, since it will not be used for implantation and there are no specific requirements for the size of the construct either. However, it is important to characterize the milled GelMA suspension bath to ease its translation to other applications in future use.

In earlier sol fraction experiments, the results were distorted due to a lack of sensitivity of the scale when weighing single 2x6mm discs in an Eppendorf tube. In a follow-up experiment, five discs were placed together in a tube per condition, to increase the weight of the sample in order to minimize the effect of the error of the scale on the experiment. Still, this weight was not sufficient and weights smaller than the initial tube weight were measured at day 1 and 2. Therefore, a relatively large volume (500 µl) of bulk and milled GelMA was pipetted into a 48 wells plate (as in the final experiment with LUHMES cells), crosslinked, and used for the sol fraction and swelling ratio analyses, which proved to be sufficient.

It was hypothesized that blending GelMA leads to less swelling and an increased loss of crosslinked polymers, because the blending cuts through chemical bonds, which may slightly damage the biomaterial. This could mean that the shape fidelity of printed constructs would be better in milled compared to bulk GelMA. However, after conducting an unpaired student's t-test, neither the sol fraction nor swelling ratio were found to be significantly different when 5% bulk and blended GelMA were compared ($p=0.1047$ and $p=0.1123$ respectively)(Fig. 5). The sol fraction of 5% GelMA has a

mean of 25.11% for bulk GelMA and 23.88% for blended GelMA (Fig. 5A), meaning that in both conditions approximately one fourth of all crosslinked polymers are lost. The swelling ratio has a mean of 13.74 for bulk and 12.32 for blended GelMA (Fig 5B), which is comparable to the swelling ratio values of Aubin *et al.* (Aubin et al. 2010), whose high DoF (81.4%) 5% bulk GelMA has a swelling ratio of 15. Indeed, when looking at Fig. 5B, it can be observed that the mass swelling ratio decreases slightly after blending the GelMA, demonstrating that the blending might have some effect on the ability of the GelMA to soak up and store liquids such as PBS or medium in its polymer network (Aubin et al. 2010). We can conclude that all samples take up a lot of PBS and thus swell considerably compared to their lyophilized form.

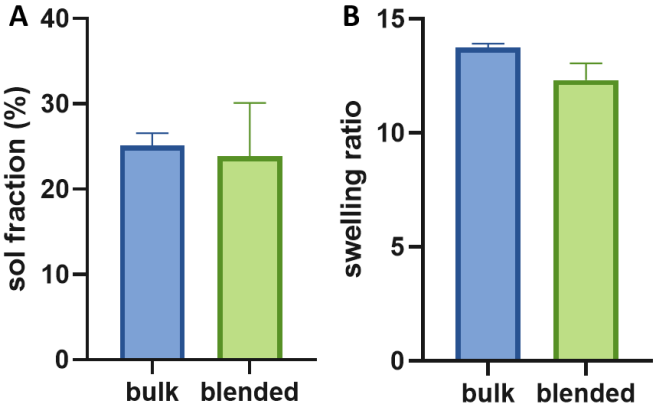

Fig. 5. A) Sol fraction and B) swelling ratio of 5% bulk GelMA as compared to 5% GelMA milled for 60s. Neither the sol fraction nor swelling ratio are significantly different when 5% bulk and blended GelMA are compared (p=0.1047 and p=0.1123 respectively). The table with the exact values can be found in Supplementary Fig. S6.

3.2 3D print parameters

Initially, the CELLINK Incredible was used to print constructs, but the RegenHU 3D Discovery provided many benefits, including being situated in a flow cabinet with UV lamp, allowing for sterility at the time of the experiment, and a larger range of print options and control. Constructs were bioprinted as depicted in Fig. 1. This shape was designed to optimize the printing parameters such as feedrate and printing pressure, by including multiple straight lines, sharp corners, and an increasing distance between filaments, to assess how far neurites projecting from neurons in the filaments would reach. For example, if the feedrate is too high, the sharp corners of the serpent shape would become round, since the bioink is printed into a suspension bath of low mechanical stiffness, instead of attaching to a flat surface. Moreover, the filament could become fragmented as it can be dragged forward by the printhead and nozzle through the suspension bath. This project did not assess the effect of needle shape and size on shape fidelity. In order to reduce the range of parameters that have an impact on printing in suspension baths to a manageable selection for the time frame of this project, the 25G needle was selected early on in the project, for its stress-reducing cone shape and inner diameter that is suitable for extruding cells.

3.3 3D bioprinting process

3.3.1 Printing hiMSC at low pressure results in good cell viability

Parameter optimization was performed for many factors involved in extrusion-based bioprinting. However, optimized parameters for a specific cell type are not necessarily translatable to another cell type (Ouyang et al. 2016), especially if they vary considerably in size and rigidity, such as hiMSCs, hESCs, and LUHMES.

To optimize the printing process including machine settings and biomaterial-related parameters involved, hiMSCs were used for the first set of experiments of this project. In the most successful experiment, they were printed in a 5% gelatin bioink at a cell density of approximately 50M cells/ml (52.6M) in a 5% GelMA suspension bath milled for 60s. The filament width at t1 or printing resolution aimed for during this project was a diameter of ≤ 400 nm to provide all cells of the filament with sufficient nutrients and oxygen and prevent the development of a necrotic core (Mattei et al. 2014; Magliaro et al. 2019). Many parameters affect the diameter of the extruded filament, including the printing pressure and feedrate, the inner diameter of the nozzle, the cross-linking kinetics, microparticle size, viscosity and fluidity of the suspension bath and the bioink, and the cell size (Hinton et al. 2015).

To assess the effect of varying feedrates and printing pressures on cell viability and resolution, livedead assays were performed on the first day after printing. Fig. 6A provides an overview of tilescans made with the Thunder microscope. These images show that printing hiMSCs at low pressure results in a good cell viability. Since GelMA is a porous biomaterial, nutrients from the medium are still accessible to cells within the construct after the suspension bath is crosslinked.

Because nutrients and oxygen can only travel ±200 µm, meaning filaments with a diameter over 400 µm can develop necrotic cores, the filament widths obtained in this experiment are not optimal (Fig. 6B). Interestingly, the filament width does not seems to decrease with increasing pressure for the same feedrate. After doing a 2-way ANOVA, no results were found to be significant. Because the feedrate or printing pressure does not significantly affect the filament width, we cannot conclude that any of these feedrates or printing pressures works better than the others.

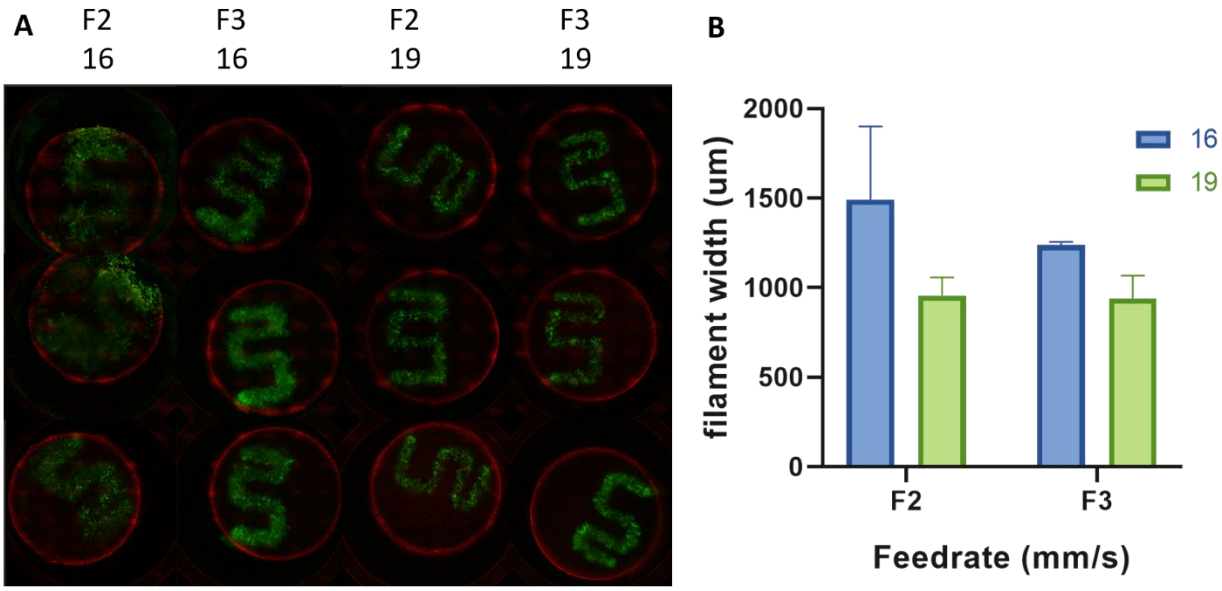

Fig. 6. A) Livedead images of hiMSCs on t1 at a 50M cells/ml cell density in a 5% gelatin bioink embedded in a 60s milled 5% GelMA suspension bath at a printing pressure of 16 kPa and 19 kPa and feedrate of 2 and 3 mm/s. B) Bar graph of filament width per condition, indicating the printing resolution (not statistically significant). The average filament width for F2 was 1492±408 µm at 16 kPa and 957±101 µm at 19 kPa and for F3 1237±20 µm at 16 kPa and 940±128 µm at 19 kPa.

During this project, it was not only attempted to create a construct of differentiated neurons that was viable post-printing, but initially the high cell density that is characteristic for the brain was also pursued. Previous papers have reported extrusion-based printing of hESC and human neural stem cells, but in these reports the cell density was rather low, ranging from 2-10M cells/ml (Gu et al.

2016; Ouyang et al. 2016; Zhou et al. 2018). To incorporate this in the bioprinting process, considerable time was spent on increasing the cell density of the bioink at the start of this project, aiming for a bioink comprising 100M cells/ml to replicate the cell density of the brain (Braitenberg 2001; Cullen et al. 2006). Inspired by the experimental set-up suggested by Jeon and colleagues, who employed crosslinkable oxidized and methacrylated alginate (OMA) microgel suspension baths to print constructs, multiple experiments with hiMSC in cell-only bioinks were performed to maximize the cell density from the start of the printing process (Jeon et al. 2019). However, after several attempts, it was acknowledged that the drawbacks of this approach significantly challenged the experimental process. Since it is difficult to obtain sufficient volume to print with (which is further hampered by dead space in the cartridge), cell-only bioinks have limited scalability, their structural integrity is low, pre-printing preparations, including culture investments such as time, space, and materials, are extensive, and the relatively high viscosity of the bioink limits extrudability, with a risk of clogging and thus a detrimental effect on the printing resolution (Khoshnood and Zamanian 2020). It was therefore decided that some biomaterial would be added to the bioink, which was likely to improve cell viability by reducing direct stress applied to the cells by cell encapsulation and support proliferation, migration, and differentiation (Malda et al. 2013). The addition of biomaterial to the bioink was especially important later on in the project, since hESC and LUHMES are delicate cell types that are easily stressed.

3.3.2 Printing hESC at low pressure results in good resolution and high cell viability

hESCs were printed using the similar conditions as the hiMSCs: they were printed in a 5% gelatin bioink at a cell density of 50M cells/ml in a 5% GelMA suspension bath milled for 60s. The printing pressure had to be increased for the proper extrusion of a sufficiently gelated bioink. Fig. 7A provides an overview of tilescans made with the Thunder microscope, showing that printing hESCs at low pressure results in a high cell viability and good resolution. As seen in the graph in Fig. 7B, which shows the filament width on t1 after printing for feedrates F2, F3, and F4, the printing resolution improves with increasing feedrate at a constant printing pressure of 40 kPa. Indeed, as theoretically and experimentally demonstrated by Prendergast *et al*. (Prendergast and Burdick 2021), filament width decreases with increasing feedrates. Between conditions, the difference in filament width was not statistically significant (p=0.24).

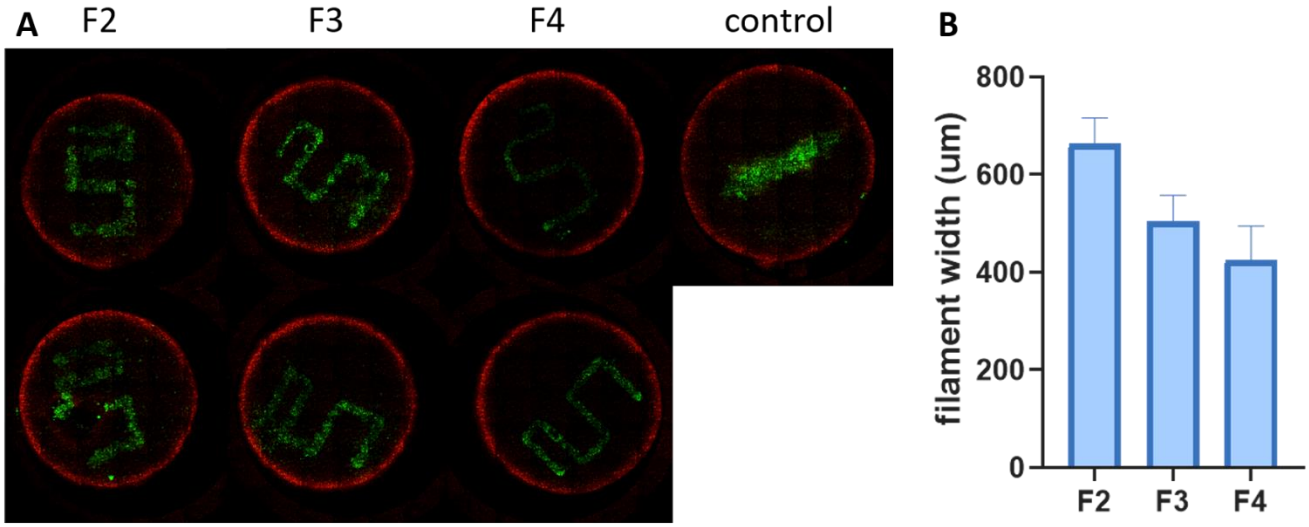

Fig. 7. A) Livedead images of hESCs on t1 at a 50M cells/ml cell density in a 5% gelatin bioink embedded in a 60s milled 5% GelMA suspension bath at a printing pressure of 40 kPa. B) Bar graph of filament width per condition indicating the printing resolution of hESC. The average filament width was 662±54 µm for F2, 504±54 µm for F3, 424±71 µm for F4 (p=0.24).

Feedrates higher than F4 resulted in dragging of the extruded filament, which resulted in disrupted filaments and thus separate populations of cells. Since the print accuracy of these samples was so low, samples printed with feedrates F4-F11 were therefore excluded from the analysis. Unfortunately, after t1, the samples prepared for live/dead analysis on t7 had to be fixated, due to a bacterial infection. From this experiment, we can conclude that a printing resolution of 400 µm can be obtained with high cell viability, which is promising for further cell culture and differentiation protocols.

The fact that feedrates higher than F4 resulted in dragging of the extruded filament, can partly be explained by the interfacial tension (the tangential force of the bioink into the suspension bath) and the lower volume of bioink that is deposited per well due to the increased speed. Moreover, the geometry of samples printed with feedrates ranging from F5-F7 was probably disturbed due to further thermal gelation of the bioink while the nozzle was immersed in the cold suspension bath (which was stored in the fridge at 4°C), requiring more pressure for extrusion.

When comparing the results of bioprinting hiMSCs and hESCs and the large difference in filament width between them, it is important to note the difference in cell size between hiMSCs (40-60 µm diameter), hESCs (13 µm diameter), and LUHMES (10 µm diameter). Because of the considerably smaller cell size of hESCs and LUHMES, the resolution was likely to improve a lot when continuing after printing hiMSCs. This also means these smaller cells will be encapsulated in more biomaterial in bioinks of a similar cell density, which may prove to be beneficial for the cell viability. Therefore, the results from printing hiMSCs provided sufficient support to continue with the second objective, which involved the use of hESCs instead of hiMSCs to bioprint viable constructs.

3.3.3 LUHMES cells printed in a gelatin bioink at high cell density form aggregates

The intended third objective consisted of viral transduction of hESCs to express neural transcription factors (a 28-day protocol) or neural induction by changing to culture medium containing specific growth factors (a protocol lasting >5 weeks)(Theka et al. 2013; Srikanth and Young-Pearse 2014). However, these long and expensive protocols would pose a large challenge for improving the printing conditions and shape fidelity of the constructs within the timeframe of the project, since obtaining results of experiments would take a significant amount of time. Therefore, instead of differentiating hESCs, the LUHMES neural cell line was used in the last part of this project. This is a human-derived neuronal cell line that is genetically modified to proliferate continuously until they are induced to differentiate into immortalized, mature dopaminergic neurons by adding tetra- or doxycycline. Because LUHMES have the ability to differentiate into TH expressing, post-mitotic, dopaminergic neurons within 5 days, they are increasingly being used in *in vitro* models for neurodegenerative diseases. These include 2D and 3D models of PD, as LUHMES respond to neurotoxins that are commonly used to induce PD and subsequently demonstrate a reduced cell viability and dopamine uptake, resulting in an increase in apoptosis (Smirnova et al. 2016; Harischandra et al. 2020; Ko et al. 2020). In this project, LUHMES cells provide a less expensive and time consuming alternative to differentiating hESCs to improve the bioink and the GelMA-based suspension baths to be suitable for (DA) neurons to establish a neural network. Furthermore, unlike hESCs and iPSCs, LUHMES produce a homogeneous population of neurons, which is useful for the optimization of the model.

The third aim of this project was to create a viable construct consisting of differentiated neurons that are connected in a 3D neural network. Up to date, only few research projects in which neural cells have bioprinted have been reported (Hsieh et al. 2015; Gu et al. 2016; Ouyang et al. 2016; Zhou et al. 2018). The authors mostly print cells that have already been induced to differentiate along the neural lineage, rather than printing stem cells that would only differentiate post-printing. Printing already differentiated cells results in increased control over the differentiating process, but requires

harvesting large cell numbers before printing because of limited proliferation, which means that at a fixed cell density for the *in vitro* model, cells are encapsulated in less material, resulting in a higher shear stress being applied to the cells. On the other hand, starting with stem cells provides the advantage of an increasing cell number post-printing due to proliferation, meaning less cells are needed in the bioink, which in turn protects the cells from shear stresses and requiring enhanced safety measures only after printing in case of using a viral transduction protocol.

A preliminary print with LUHMES cells using the printing parameters and conditions of the hiMSC and hESC prints was conducted. For this purpose, a pellet of LUHMES cells was resuspended in a 5% gelatin bioink at a cell density of 25M cells/ml, due to low cell numbers after harvesting. The bioink was gelated in a water bath at 25 °C for 30 mins, which resulted in a properly gelated bioink, and extruded into a 5% GelMA suspension bath milled for 60s. The printing pressure required for extrusion was 74 kPa and the feedrate was set at F3. To save materials such as Matrigel, LUHMES culture supplements and antibodies, 48 instead of 24 wells plates were used.

LUHMES printed in gelatin formed large aggregates directly after printing (Fig. 8). Furthermore, over two weeks of time, they did not extend any neurites at all. These results correspond with previous experiments that also showed that neural cells did not grow well in GelMA and formed large aggregates (unpublished data, M. Caiazzo). Images obtained with the Thunder microscope after immunostaining were of low quality and showed weak stainings of βIII-tubulin, TH, and DAPI. Therefore, the immunocytochemistry protocol for staining cells in 3D was further improved, since the cells are encapsulated in crosslinked GelMA, making it more difficult for the relatively large proteins and antibodies used in this procedure to reach the cells.

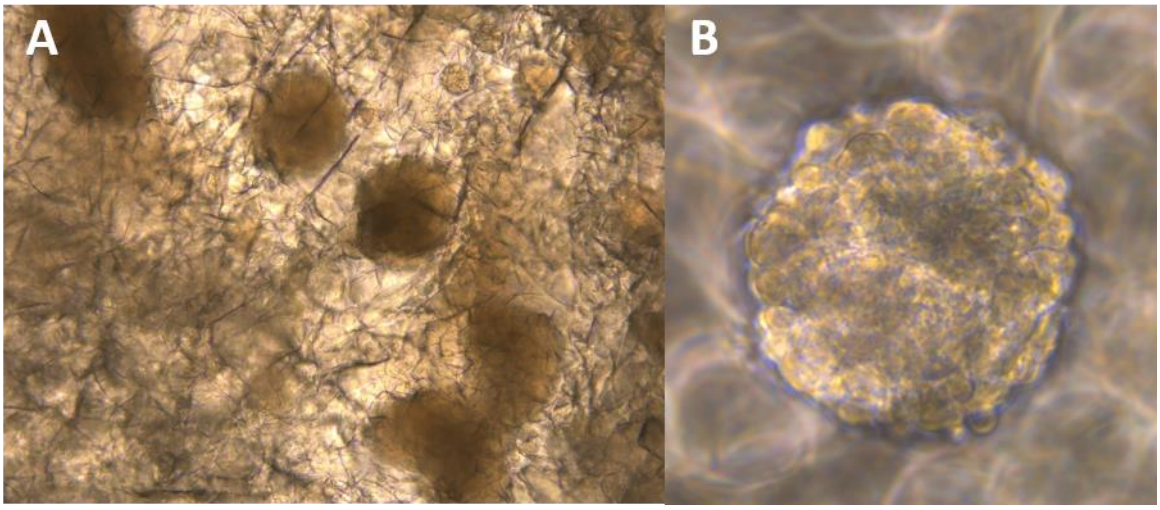

Fig. 8. LUHMES cells (t4) printed in a 5% gelatin bioink at a cell density of 25M cells/ml into a 5% GelMA suspension bath milled for 60s form large aggregates A) 5x objective B) 40x objective.

Based on the results obtained during this testprint, it was hypothesized that the formation of aggregates could be mainly due to two factors. Firstly, the LUHMES were printed in a bioink consisting of gelatin, which, as a sacrificial material, liquefies when warm medium is added to the samples. This meaning that the cells are thus present in an empty channel upon incubation and have no material to attach to anymore. In certain applications, such as the creation of vasculature, this is desirable (Kolesky et al. 2014), but in this case it results in cells attaching to each other instead of to their surrounding biomaterials. Secondly, the high cell density and the 'stickiness' of the LUHMES cells could result in aggregate formation, as they tend to cluster together in large numbers and are difficult to separate by resuspension. Moreover, LUHMES could aggregate due to the stress they are exposed to during the printing process, for example because by the long time in suspension before

printing or the printing conditions, including the shear stress from being extruded through a nozzle (although LUHMES cells in a gelatin bioink that were manually pipetted also formed aggregates), or the GelMA concentration which may be too high (Aubin et al. 2010).

3.4 Neuronal Differentiation Studies using Immunocytochemistry

3.4.1 LUHMES cells in milled GelMA suspensions with Matrigel and fibronectin form neurites

The results of this preliminary experiment show that, instead of forming aggregates, LUHMES cells resuspended in the 5% milled GelMA suspension bath that was milled for 60s with Matrigel alone (11,2 µl/ml), but even more so in the condition with Matrigel (11,2 µl/ml) as well as fibronectin (50 µl/ml), form neurites towards each other in 3D at a cell density of 20M cells/ml. In sharp contrast, in the GelMA only or GelMA with fibronectin (50 µl/ml) conditions, aggregates have formed again and no neurites were visible at all. The cell density of the bioink (20M cells/ml), seemed quite high. Longer neurites were mostly visible in areas with lower cell densities, stretching up to 250 µm. In all conditions, many cells washed out of the crosslinked suspension bath.

In this experiment, in order to avoid the formation of aggregates of LUHMES and stimulate neurite outgrowth, different biomaterials were added to the milled GelMA to provide a more suitable microenvironment with structural, ECM-like attachment peptides and cell binding motifs for support. This particle reinforced hydrogel should stimulate the cells to form neurites and stretch out, instead of clustering together. Although GelMA contains many cell binding sites on all of its polymer chains, not all cells are able to bind these binding sites (Aubin et al. 2010). Therefore, cell adhesion, elongation and migration might improve for certain cells by adding binding motifs to the milled GelMA.

Unpublished preliminary results from S. Bahtiri and B. Qiu showed that LUHMES cells grown in culture plates coated with laminin form aggregates, whereas those cultured on wells coated with Matrigel or fibronectin proliferate extensively and form neurites. Their data suggests that LUHMES require certain ECM-like elements in order to attach and spread instead of aggregating. Building on these results, the addition of Matrigel and fibronectin to the GelMA slurry was assessed.

Fibronectin is a natural ECM material that provides adhesion proteins that can complement the in GelMA abundant RGD and GFOGER motifs for focal adhesion (Yue et al. 2015; Lavrentieva et al. 2019). It plays an important role in the development of axons (Rutishauser 1993), has been extensively used for peripheral nerve regeneration (Tong et al. 1994; Ahmed and Brown 1999; Chen et al. 2000) and has been shown to induce neurites to align by contact guidance as fibers (Ahmed and Brown 1999). Matrigel is a basement membrane preparation that is used to mimic the ECM, which is harvested from Engelbreth-Holm-Swarm (EHS) mouse sarcomas. These tumors are rich in ECM proteins such as laminin, collagen, and a variety of growth factors (Kleinman et al. 1982; Slater et al. 2018). Matrigel is fluid at 4°C, gelates above 10°C and is often used in stem cell culture to coat polystyrene wells. Since its polymerization is not reversible, its temperature should be tightly controlled (Slater et al. 2018). Matrigel can be diluted in medium to obtain a low mechanical stiffness. Concentrations of 4.4, 8, and 17 mg/ml demonstrated stiffnesses of 20, 70, and 300 Pa respectively (Chaudhuri et al. 2014).

The results of this preliminary experiment were very promising as they show that LUHMES cells resuspended in the 5% milled GelMA suspension bath that was milled for 60s with Matrigel alone (11,2 µl/ml) and Matrigel (11,2 µl/ml) and fibronectin (50 µl/ml) form neurites in 3D. The cell density of the bioink (20M cells/ml) seemed quite high, which could leave the cells with less space and less of a need to extend neurites to each other, since potentially many of them are in direct contact in large populations already. It should be noted that in all conditions, many cells were washed out of the

slurry onto the bottom of the well. This could be due to the high cell density of the suspensions in combination with their small size (10 µm diameter), resulting in them being washed out of the slurry more frequently compared to lower cell densities.

Even though this experiment set out to improve the GelMA suspension bath, the milled GelMA with supplements could be used as a bioink too. Using a bioink consisting of GelMA instead of gelatin could help to stimulate contact guidance (Fan et al. 2012). Since the cells in the milled GelMA with Matrigel and Matrigel and fibronectin conditions formed neurites in 3D, it could be a good alternative to gelatin used in the bioink in previous experiments. Furthermore, using a completely new biomaterial for the bioink instead of gelatin could change the mechanical properties of the suspension bath and bioink considerably, thus complicating the optimization process.

3.4.2 LUHMES cells in milled GelMA suspensions form neurites at different cell densities

The results of the second preliminary experiment show that in all conditions ranging from 10-25M cells/ml, neurites have formed in 3D. On day 8 and 12 after printing, thus on day 10 and 14 of differentiation respectively, LUHMES neurons stain positive for βIII-tubulin and some samples also for TH, although the latter was not that successful. It was visible that the overall cell density is still quite high, but that in cell-dense areas many neurites of ±200 µm have developed. In areas of a lower cell density, longer neurites have formed. In all conditions, many cells were washed out of the suspension bath onto the bottom of the well, where some continued growing. No considerable differences between samples fixed on day 8 and 12 could be observed.

Building on the results from the previous experiment with LUHMES cells, the second preliminary experiment was performed to determine the most appropriate cell density for the bioink. It was hypothesized that decreasing the cell density from 20M cells/ml would result in the formation of longer neurites by providing them with more space, and that increasing the cell density would lead to the formation of a higher number of short neurons. Therefore, a dilution of cell densities was prepared to see which conditions would be most appropriate for our model, ranging from 10-25M cells/ml.

During differentiation, the medium of the samples changed color very rapidly, which could indicate a cell number that was too large for the amount of nutrients provided. Therefore, the concentration of the differentiation medium supplements was adjusted, considering the indicated concentration was meant for the total volume of the well, which consists of the volume of the added medium, but also the volume of the crosslinked suspension bath. Thus, the volume of the supplement to be added should be calculated per total volume, which in most cases almost doubles the amount of supplement that was added (Appendix). Moreover, more attention was paid to the expiry date of supplements, which often only last one week after thawing.

To demonstrate proof of neuronal differentiation and dopaminergic maturation, the immunocytochemistry protocol for staining 3D samples was adjusted, now comprising longer incubation times and washing steps, because it takes longer for the relatively large proteins and antibodies used in this procedure to reach the cells due to the their encapsulation in crosslinked GelMA. Tyrosine Hydroxylase or TH was stained as a marker of dopaminergic neurons, because it is an enzyme that catalyzes the conversion of L-tyrosine to levodopa for dopamine secretion. TH is mostly present on the cell membrane and in the cytosol near neuron vesicles and mitochondria. The expression of TH marks the ability of a cell to synthesize dopamine (Daubner et al. 2011). βIII-tubulin (TUBB3 or TUJ1), on the other hand, is a specific marker of class-III maturing neurons, as it is a microtubule element that comprises a major part of the cytoskeleton in differentiating neurons (Caccamo et al. 1989; Kapitein and Hoogenraad 2015; Harischandra et al. 2020). Because of their small diameter, individual neurites are impossible to visualize with fluorescence microscopy (Dent

and Baas 2014). However, since dendrites and axons are present in tubes of a few microns in diameter that contain tightly packed bundles of microtubules, βIII-tubulin can visualize a group of neurites, to indicate the progress of neural network development established for neuronal signaling (Caccamo et al. 1989; Kapitein and Hoogenraad 2015; Harischandra et al. 2020). Without dynamic microtubules expressing βIII-tubulin, neurons would not be able to carry out necessary cellular processes such as the transport of signals (Katsetos et al. 2003).

The results of this experiment 8 days after printing, were promising as they show that many LUHMES stain positive for neuronal markers (βIII-tubulin), and in certain cases also for mature dopaminergic markers (TH). Most cells are likely not to be mature however. Of note, LUHMES can be fully differentiated and mature already at 2 or 3 times their cell body length (20-30 µm), and some neurites measured in this experiment are 250 µm (unpublished data Caiazzo). Whether the cells are mature and actually connected in a network should be proved in future experiments by calcium imaging, which is a technique to localize and measure basic physiological neural functionality, since electrical activity in neurons is initiated by an influx of Ca^{2+} (Iosub et al. 2015; Wei et al. 2020). If the cells are connected in a neural network or circuit, calcium signaling moves through a cultured plate or construct resembling a wave (Iosub et al. 2015). Since it can distinguish between excitatory and inhibitory neurons, it is a useful tool to study the neural circuitry *in vitro* as well as *in vivo*. Another option would be to do an electrophysiology assay or to place the construct on a multielectrode array which can transmit or receive neural signals with its microelectrodes, to determine if the neurons are able to fire (Wei et al. 2020). Unfortunately there was not time for these experiments during this project.

All cell densities could be too high, resulting in cells clustering together, but this might also be due to the fact that LUHMES often cluster together. The high cell densities used in this experiment probably leads to the formation of more short neurons. At a lower cell densities, it is likely that longer neurites will form, because they need to extend more to establish contact with each other. It depends on the outlook whether short or long neurites are desirable for the model.

Since the DAPI was overstained considerably, the 3 hrs incubation period was reduced again. This is understandable, since the pores of the crosslinked GelMA should be large enough for penetration by smaller molecules such as DAPI, as well as the ethidium homodimer and Calcein-AM used in the live/dead protocol, unlike the larger molecules used as primary and secondary antibodies. Because of using the Leica Confocal instead of the Thunder, and because samples were placed on a thin glass slide instead of being present in well plates with thick bottoms during imaging, the images looked significantly better compared to the ones obtained after the testprint.

Because the results of this experiment are not entirely clear, but look promising, it was decided to move on to the next experiment in which LUHMES were bioprinted. Since the two preliminary experiments showed that LUHMES resuspended in milled GelMA with Matrigel and fibronectin are able to differentiate and form neurites, the same material was used for the suspension bath as well as for the bioink, to replace gelatin and provide LUHMES with structural elements they can attach to and form their neurites along after printing.

3.5 LUHMES print

3.5.1 Bioprinting of LUHMES results in high cell viability

On day 1 and 7 after printing, live/dead assays were performed to evaluate the cell viability and mean filament width. For this purpose, 2 of every 4 samples per feedrate (F3-F6) as well as the 2 manually pipetted control samples were assessed. Although the deposition of bioink appeared successful, it could be observed already shortly after printing, that cells had dispersed throughout the

suspension bath instead of forming a filament. Therefore, the filament width and thus printing resolution could not be calculated. No structural similarity between the G-code and the printed construct could be observed.

The cell viability of printed LUHMES on day 1 was 78.6±6.7%, which indicates that limited harm was done to the cell by the printing process, resulting in high cell survival post-printing (Fig. 9A). Control samples that consisted of bioink that was manually pipetted into the suspension baths demonstrated a slightly higher cell viability of 82.8±6.3%. However, the cell viability was not found to be statistically significant (p=0.43). On day 7, most cells were still alive (Fig. 9B). However, the cell viability could not be quantified because the live cells were differentiated and clustered together and thus single cells could not be distinguished from one another as single cells (as opposed to the single cells that could easily be counted on day 1). From these results we can conclude that this extrusion-based printing process does not harm LUHMES cells considerably and that the cell viability is high.

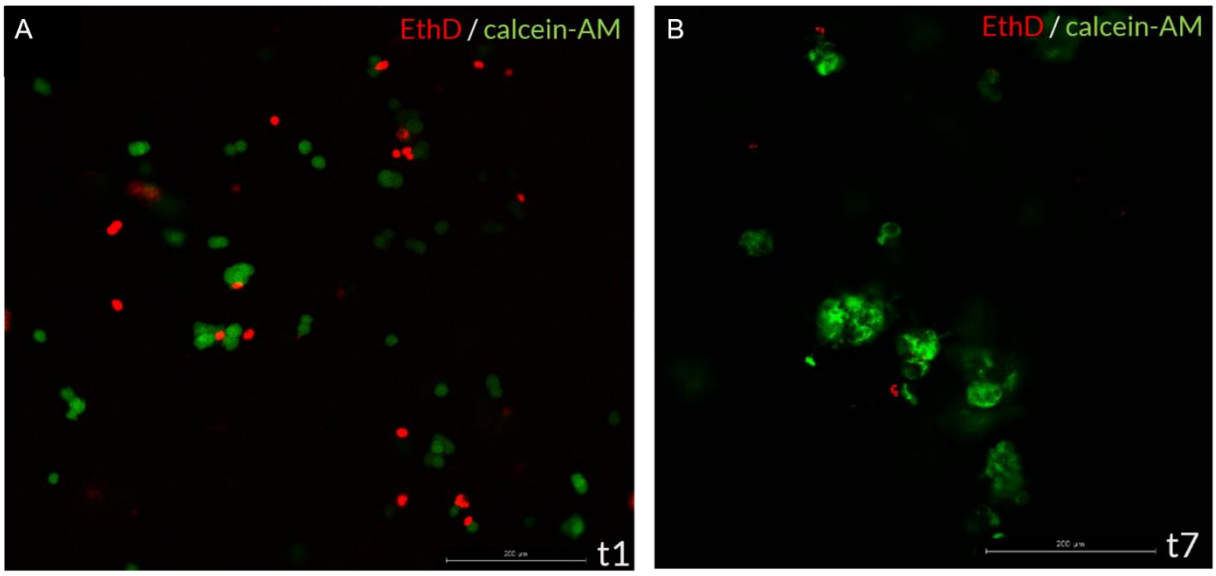

Fig. 9. Cell viability of bioprinted LUHMES cells at a cell density of 10M cells/ml printed in a 5% GelMA bioink milled for 60s with Matrigel (11,2 µl/ml) and fibronectin (50 µl/ml) embedded into a 5% GelMA suspension bath milled for 60s with Matrigel (11,2 µl/ml) and fibronectin (50 µl/ml) at a printing pressure of 13 kPa on A) t1 and B) t7. Images of live/dead staining obtained with Confocal fluorescence microscopy (200 µm scale bars).

The dispersion of cells could be due to the fact that the bioink was not sufficiently gelated at the time of extrusion, as the bioink was extruded directly after the cartridge was loaded in order to prevent the cells from getting stressed and harmed by low temperatures in the fridge. Gelation at room temperature would not be possible, since the milled GelMA slowly starts to dissolve when the temperature increases after it has been taken out of the fridge and not kept on ice. However, according to the literature (Hinton et al. 2015; Prendergast and Burdick 2021) and previous experience, printing a bioink with a low viscosity should not pose a large problem because of using the suspension bath. One possible explanation is that the LUHMES did disperse throughout the bath because of their very small size, with a diameter of 10 µm as compared to diameters as wide as 60 µm for hiMSCs, meaning they could potentially penetrate through the pores of the GelMA suspension bath during and after printing, instead of being kept in place by the bath. When a test print with the same printing parameters and biomaterials was conducted with hiMSCs instead of LUHMES cells as a control, the hiMSCs did not spread widely through the suspension bath, but were mostly present in the printing path as described by the G-code, resulting in a high print accuracy. Indeed, hiMSCs are much larger than LUHMES and are unlikely to penetrate through the pores of the GelMA suspension bath. To prevent the cells of the bioink from dispersing throughout the

suspension bath to improve the shape fidelity and resolution, the bioink and suspension bath should be improved in future experiments.

One option is to implement a thermal gelation step after loading the cartridge to ensure printing with a properly gelated bioink (Ouyang et al. 2016). In our project this would mean thermally gelating the cartridge with cells resuspended in gelatin or milled GelMA with fibronectin and Matrigel in the fridge at 4°C or in a water bath at a low temperature. It should be noted that thermal gelation at temperatures that are too low can result in over-gelation, as described by the printability characteristic (Ouyang et al. 2016). Printing with an over-gelated bioink results in interrupted filament morphology, which should be prevented for its detrimental effects on the geometry and mechanical properties of the construct (Ouyang et al. 2016; Schwab et al. 2020). Moreover, low temperatures might cause harm to delicate cell types, such as hESCs (Ouyang et al. 2016). Another option to improve the shape fidelity and resolution, is by increasing the concentration of the GelMA in the suspension bath. However, a suspension bath of a higher mechanical stiffness would probably be a limiting factor for the formation of neurites, whereas neurite outgrowth should be stimulated.

After improving the shape fidelity and cell retention, the most appropriate cell density should be determined. During this process, it should be taken into consideration whether a high number of short neurites or a lower number of longer neurites is preferred. Printing with a cell density lower than 10M cells/ml should be evaluated, since this might give neurons more space to form neurites.

One possible solution to still assess the cell viability for this experiment would be to quantify the green (live) versus the red (dead) area, but since the living cells are much larger compared to the shrunken dead cells, this would not give an accurate representation of the cell viability. The cell viability based on these images is likely to be an underestimation, because dead cells have washed out of the crosslinked suspension bath to end up on the bottom of the wells.

3.5.2 Bioprinted LUHMES cells form neurites in 3D

To demonstrate proof of neuronal differentiation and dopaminergic maturation, samples were fixed at t8 and stained to detect the presence of βIII-tubulin, TH, and DAPI, using an updated immunocytochemistry protocol for staining 3D samples, which consisted a shorter incubation period of DAPI compared to the last experiments. The results show that the bioprinted LUHMES have formed many neurites that are growing across multiple planes (Fig. 10). The LUHMES seem to form clusters of cells again, instead of being present as single cells that reach out to each other with their neurites, despite the low cell density of 10M cells/ml. However, these clusters do form neurites, which they extend to one another, thus forming what looks like a network.

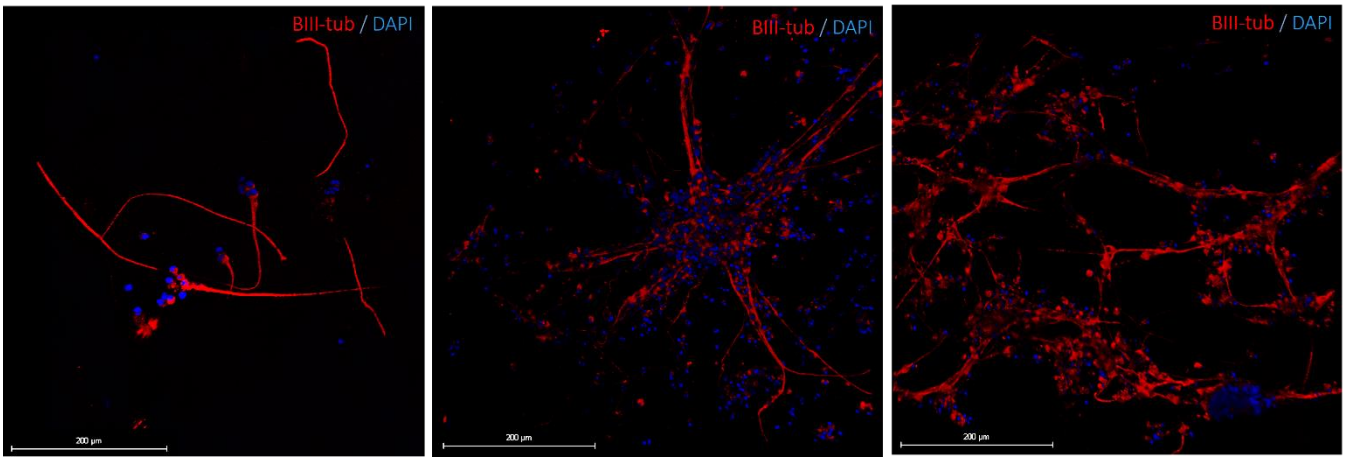

Fig. 10. Immunocytochemistry images of LUHMES cells at t8 at a cell density of 10M cells/ml. These LUHMES, printed in a 5% GelMA slurry bioink milled for 60s with Matrigel (11,2 µl/ml) and fibronectin (50 µl/ml) embedded into a 5% GelMA suspension bath milled for 60s with Matrigel (11,2 µl/ml) and fibronectin (50 µl/ml) at a printing pressure of 13 kPa, form neurites in 3D (scale 200 µm).

Although it is hard to determine where neurites begin and end based on the above images, some stretch from 50 µm to at least 250 µm between clusters of nuclei. In areas with a low cell density, less neurites are visible, but some of these reach distances up to 700 µm. Again, as in the preliminary experiments with LUHMES suspended in milled GelMA, many cells washed out of the suspension bath onto the bottom of the well.

The results of this experiment are very promising, as they show that bioprinted LUHMES can form neurites that are growing omnidirectionally in large numbers (Fig. 10). It seems that a high cell density results in the formation of a large number of relatively small neurites, whereas a lower cell density results in the formation of a smaller number of much longer neurites. It can be observed that the LUHMES continue to form clusters despite the low cell density. One reason they aggregate might be the small diameter of the nozzle. However, aggregation can also be seen in the samples pipetted by hand, of which the pipet tip diameter is considerably larger, and changing to a nozzle with a bigger diameter is likely to negatively affect the printing resolution.

In the field of biofabrication, it is important to consider mechanical properties and morphology, as well as functionality (Levato et al. 2020). In order to create a well-functioning neural network, this means not only shape fidelity and cell viability of neural cells should be pursued, but also maturation and dopamine secretion. However, because of time constraints at the end of this project, neuronal differentiation was only assessed by immunostaining. As this immunocytochemistry protocol provides no proof for functionality, it is still a bit early to call this a neural network. However, the formation of neurites that are growing towards each other in 3D and stretch over small as well as large distances are very promising results to continue to explore for the development of a 3D *in vitro* neural network.

4. Conclusions

The aim of this project was to establish a 3D *in vitro* neural network to study Parkinson's disease by suspended extrusion-based bioprinting of a cell-laden bioink. Therefore, the project was divided in three objectives: i) developing a suitable suspension bath to print a viable construct (designed to study PD) using hiMSCs to optimize the printing process ii) developing a viable construct using hESCs, which can be differentiated into neurons induced by a growth factor protocol or viral transfection and which closely resemble iPSCs, and iii) developing a viable construct of cells differentiated into neurons connected in a 3D neural network.

To summarize, we can conclude that the milled GelMA suspension bath is a promising tool in the field of biofabrication. By varying the GelMA concentration and blending time, the physical, mechanical, and swelling properties of GelMA can be finely tuned for the desired application: in this case a hydrogel that is suitable for use as a suspension bath, that is crosslinkable, and whose mechanical stiffness is very low. During this project, it was shown that 5% GelMA milled for 60s results in a suspension bath that is suitable to print hiMSC at a high cell viability and shape fidelity and hESCs at a high cell viability and a high resolution of 400 µm. Moreover, this project also demonstrated that the 5% GelMA milled for 60s to which Matrigel and fibronectin were added to provide more cell binding motifs, was a suitable suspension bath for extrusion-based bioprinting of LUHMES cells at high cell viability, and that these cells underwent neuronal differentiation and formed a network of neurites in 3D over a week of culture. Nonetheless, proof of maturation and functionality of the potentially in a neural network connected neurites by calcium imaging, electrophysiology, and additional immunofluorescence assays that stain for synaptic markers is still required.

Based on the results of this project, we can conclude that suspended extrusion-based bioprinting of LUHMES cells in a soft, milled GelMA suspension bath reinforced with Matrigel and fibronectin, followed by neuronal differentiation, results in 3D growth of neurites that may form a neural network. This easily accessible and widely applicable approach to bioprinting soft materials can be employed to develop more advanced PD *in vitro* models in the future, for disease modeling, drug-screening and drug-discovery.

5. Future Outlook

For further characterization of the model and proof of neuronal differentiation, more quantitative methods such as flow cytometry, qPCR, electrophysiology and calcium imaging should be employed. Moreover, the presence of synaptic markers should be assessed. These markers visualize synapses, which are vital for the functionality of a neural network and are indicative of maturation (Kapitein and Hoogenraad 2015; Thomas and Willerth 2017; Kim et al. 2019; Qiu et al. 2020). Furthermore, ELISAs and Western Blots can be performed to measure dopamine and TH levels (Scholz et al. 2011; Fauss et al. 2013). This may provide interesting outputs when the diseased model of a neural network has been established, since the degeneration of DA neurons may be further elucidated by studying their metabolism.

For the purpose of improving the formation of neurites and elongation of neural cells throughout the bioink and suspension bath, cell adhesion studies can be performed. These might help to assess and optimize the bioink and suspension bath, as they provide an insight in the ability of cells to bind the biomaterials that are present, which is of high importance for cell survival and cell function, especially regarding cells that function by signaling via neurites extending omnidirectionally. Chemoattractants were outside the focus area of this study, but these can also be further explored in future research, for example by being incorporated in the hydrogel of choice.

In this project, LUHMES cells provided a less expensive and time consuming alternative to differentiating hESCs to optimize the bioink and suspension baths as suitable for neural network formation. However, after finishing this project, the question remains whether stem cells can also be deposited by extrusion-based bioprinting to form a network of viable neurons after a growth factor or viral transduction protocol with neurites extending in the milled GelMA suspension baths, as was initially intended. This should be elucidated in future projects. Eventually, iPSCs are the most interesting cell type for developing a 3D *in vitro* model of PD, as it can then be made patient-specific for both personalized disease modelling and drug screening by using patient-derived cells, without needing to perform invasive biopsies or post-mortem autopsies (Benam et al. 2015; Bolognin et al. 2019). In 3D cultures of patient-derived iPSCs differentiated into human neuroepithelial stem cells, disease- and 3D-specific phenotypes of PD can be observed, including decreased TH-positive DA neuron differentiation, network and branching complexity, a reduction in the number of mitochondria, and increased cell death in neurons with the LRRK2-G2019S mutation (a common mutation in autosomal-dominant PD). Strikingly, in 2D cultures, these alterations could not be observed (Bolognin et al. 2019). In order to create bioprinted 3D patient-specific models, iPSCs can be differentiated into cell type desired for the study, although recent articles have also reported direct conversion of already differentiated cells into specialized cells of another lineage, not only at a higher efficiency but also requiring shorter differentiation protocols (Caiazzo et al. 2015). iPSCs can also be genetically edited, for example by CRISPR/Cas9 technology to correct or insert genes. It is possible that, for genetic variants of PD, TALEN- or CRISPR-mediated gene corrections may rescue the disease phenotype *in vitro*. Neurons derived from hESCs and iPSCs have already been used in PD models (Srikanth and Young-Pearse 2014) and should be further explored in the context of biofabrication.

To further advance the neural network to study PD, multiple cell types should be included in the model to mimic the cytoarchitecture of the nigrostriatal pathway, consisting of DA neurons of the substantia nigra pars compacta with axons projecting to and forming synapses with GABAergic neurons of the striatum (Qiu et al. 2020). A future coculture model can for example comprise of bioprinted DA and GABAergic neurons, and potentially even include astrocytes in the surrounding suspension bath to mimic the brain microenvironment.

Moreover, because this study used a versatile and highly tunable GelMA suspension bath that is crosslinkable by UV light, extrusion-based bioprinting can be converged with volumetric bioprinting. Instead of crosslinking a full well plate with a UV lamp, a volumetric printer provides the ability to crosslink only a specific part of the suspension bath. This can be used to embed a vessel-mimetic channel (Levato et al. 2021) of a certain biomaterial or cell type within a larger volumetrically bioprinted construct for example (unpublished data, Ribezzi 2022). This convergence of techniques not only advances extrusion-based bioprinting by providing control over the crosslinked structure around the extruded construct, but also advances volumetric bioprinting by allowing the development of multimaterial cell-laden constructs in a cell-friendly bioresin.

Another future study could develop and characterize gelatin norbornene (GelNOR)-based suspension baths for extrusion-based bioprinting. Compared to GelMA, GelNOR is a more cell-friendly gelatin derivative with norbornene instead of methacryloyl groups (Mũnoz et al. 2014). GelNOR crosslinks 10 times faster, reducing crosslinking times from minutes to seconds, which results in less UV exposure for cells and thus less cell damage, and increased control over mesh size and resolution (Mũnoz et al. 2014; van Hoorick et al. 2020; Levato et al. 2021). This means a hydrogel with smaller pores can be obtained compared to GelMA, which might keep the cells of a bioprinted construct in place even more.

Acknowledgments

I would like to thank the members of the Levato and Malda group of the Orthopaedics department of the UMC Utrecht and the Caiazzo group at the Biopharmaceutics department of Utrecht University for their contributions. In particular, my daily supervisor D. Ribezzi, my supervisors R. Levato and M. Caiazzo, B. Qiu and A. Mensinga for providing training and cells for my experiments. Last but not least, I would like to thank my parents, my sister and my partner. This project would not have been possible without your support.

References

Ahmed Z, Brown RA. 1999. Adhesion, alignment, and migration of cultured Schwann cells on ultrathin fibronectin fibres. Cell Motil. Cytoskeleton 42:331–343.

Aubin H, Nichol JW, Hutson CB, Bae H, Sieminski AL, Cropek DM, Akhyari P, Khademhosseini A. 2010. Directed 3D cell alignment and elongation in microengineered hydrogels. Biomaterials 31:6941–6951.

Azevedo FAC, Carvalho LRB, Grinberg LT, Farfel JM, Ferretti REL, Leite REP, Filho WJ, Lent R, Herculano-Houzel S. 2009. Equal numbers of neuronal and nonneuronal cells make the human brain an isometrically scaled-up primate brain. J. Comp. Neurol. 513:532–541.

Benam KH, Dauth S, Hassell B, Herland A, Jain A, Jang KJ, Karalis K, Kim HJ, MacQueen L, Mahmoodian R, et al. 2015. Engineered in vitro disease models. Annu. Rev. Pathol. Mech. Dis. 10:195–262.

Bolognin S, Fossépré M, Qing X, Jarazo J, Ščančar J, Moreno EL, Nickels SL, Wasner K, Ouzren N, Walter J, et al. 2019. 3D Cultures of Parkinson's Disease-Specific Dopaminergic Neurons for High Content Phenotyping and Drug Testing. Adv. Sci. 6:1–14.

Braitenberg V. 2001. Brain size and number of neurons: An exercise in synthetic neuroanatomy. J. Comput. Neurosci. 10:71–77.

Caccamo D V., Herman MM, Frankfurter A, Katsetos CD, Collins VP, Rubinstein LJ. 1989. An immunohistochemical study of neuropeptides and neuronal cytoskeletal proteins in the neuroepithelial component of a spontaneous murine ovarian teratoma. Primitive neuroepithelium displays immunoreactivity for neuropeptides and neuron-associated β-tubul. Am. J. Pathol. 135:801–813.

Caiazzo M, Giannelli S, Valente P, Lignani G, Carissimo A, Sessa A, Colasante G, Bartolomeo R, Massimino L, Ferroni S, et al. 2015. Direct conversion of fibroblasts into functional astrocytes by defined transcription factors. Stem Cell Reports 4:25–36.

Casey JR, Grinstein S, Orlowski J. 2010. Sensors and regulators of intracellular pH. Nat. Rev. Mol. Cell Biol. 11:50–61.

Chaudhuri O, Koshy ST, Branco Da Cunha C, Shin JW, Verbeke CS, Allison KH, Mooney DJ. 2014. Extracellular matrix stiffness and composition jointly regulate the induction of malignant phenotypes in mammary epithelium. Nat. Mater. 13:970–978.

Chen YS, Hsieh CL, Yao CH. 2000. Peripheral nerve regeneration in silicone rubber chambers filled with collagen, laminin and fibronectin. Annu. Int. Conf. IEEE Eng. Med. Biol. - Proc. 4:2561–2563.

Compaan AM, Song K, Huang Y. 2019. Gellan Fluid Gel as a Versatile Support Bath Material for Fluid Extrusion Bioprinting. ACS Appl. Mater. Interfaces.

Cooke ME, Rosenzweig DH. 2021. The rheology of direct and suspended extrusion bioprinting. APL Bioeng. 5.

Cullen DK, Vukasinovic J, Glezer A, LaPlaca MC. 2006. High cell density three-dimensional neural co-

cultures require continuous medium perfusion for survival. Annu. Int. Conf. IEEE Eng. Med. Biol. - Proc.:636–639.

Daubner SC, Le T, Wang S. 2011. Tyrosine Hydroxylase and Regulation of Dopamine Synthesis. Arch. Biochem. Biophys. 508:1–12.

Dent EW, Baas PW. 2014. Microtubules in neurons as information carriers. J. Neurochem. 2:235–239.

Engler AJ, Sen S, Sweeney HL, Discher DE. 2006. Matrix Elasticity Directs Stem Cell Lineage Specification. Cell 126:677–689.

Fan Y, Xu F, Huang G, Lu TJ, Xing W. 2012. Single neuron capture and axonal development in three-dimensional microscale hydrogels. Lab Chip 12:4724–4731.

Fauss D, Motter R, Dofiles L, Rodrigues MAV, You M, Diep L, Yang Y, Seto P, Tanaka K, Baker J, et al. 2013. Development of an enzyme-linked immunosorbent assay (ELISA) to measure the level of tyrosine hydroxylase protein in brain tissue from Parkinson's disease models. J. Neurosci. Methods 215:245–257.

Flanagan LA, Ju Y-E, Marg B, Osterfield M, Janmey PA. 2002. Neurite branching on deformable substrates. Neuroreport 13:2411–2415.

Green MA, Bilston LE, Sinkus R. 2008. In vivo brain viscoelastic properties measured by magnetic resonance elastography. NMR Biomed. 21:755–764.

Gu Q, Tomaskovic-Crook E, Lozano R, Chen Y, Kapsa RM, Zhou Q, Wallace GG, Crook JM. 2016. Functional 3D Neural Mini-Tissues from Printed Gel-Based Bioink and Human Neural Stem Cells. Adv. Healthc. Mater. 5:1429–1438.

Harischandra DS, Rokad D, Ghaisas S, Verma S, Robertson A, Jin H, Anantharam V, Kanthasamy A, Kanthasamy AG. 2020. Enhanced differentiation of human dopaminergic neuronal cell model for preclinical translational research in Parkinson's disease. Biochim. Biophys. Acta - Mol. Basis Dis. 1866:165533.

Harris G, Hogberg H, Hartung T, Smirnova L. 2017. 3D differentiation of LUHMES cell line to study recovery and delayed neurotoxic effects. Curr. Protoc. Toxicol. 2017:1–42.

Henchcliffe C, Flint Beal M. 2008. Mitochondrial biology and oxidative stress in Parkinson disease pathogenesis. Nat. Clin. Pract. Neurol. 4:600–609.

Herculano-Houzel S. 2009. The human brain in numbers: A linearly scaled-up primate brain. Front. Hum. Neurosci. 3:1–11.

Hinton TJ, Jallerat Q, Palchesko RN, Park JH, Grodzicki MS, Shue HJ, Ramadan MH, Hudson AR, Feinberg AW. 2015. Three-dimensional printing of complex biological structures by freeform reversible embedding of suspended hydrogels. Sci. Adv. 1.

van Hoorick J, Dobos A, Markovic M, Gheysens T, van Damme L, Gruber P, Tytgat L, van Erps J, Thienpont H, Dubruel P, et al. 2020. Thiol-norbornene gelatin hydrogels: Influence of thiolated crosslinker on network properties and high definition 3D printing. Biofabrication 13.

Hsieh FY, Lin HH, Hsu S hui. 2015. 3D bioprinting of neural stem cell-laden thermoresponsive

biodegradable polyurethane hydrogel and potential in central nervous system repair. Biomaterials 71:48–57.

Imamura M, Ozawa E. 1998. Differential expression of dystrophin isoforms and utrophin during dibutyryl-cAMP-induced morphological differentiation of rat brain astrocytes. Proc. Natl. Acad. Sci. U. S. A. 95:6139–6144.

Iosub R, Avitabile D, Grant L, Tsaneva-Atanasova K, Kennedy HJ. 2015. Calcium-induced calcium release during action potential firing in developing inner hair cells. Biophys. J. 108:1003–1012. Jankovic J. 2008. Parkinson's disease: Clinical features and diagnosis. J. Neurol. Neurosurg. Psychiatry 79:368–376.

Jeon O, Lee Y Bin, Jeong H, Lee SJ, Wells D, Alsberg E. 2019. Individual cell-only bioink and photocurable supporting medium for 3D printing and generation of engineered tissues with complex geometries. Mater. Horizons 6:1625–1631.

Kapitein LC, Hoogenraad CC. 2015. Building the Neuronal Microtubule Cytoskeleton. Neuron 87:492–506.

Katsetos CD, Legido A, Perentes E, Mörk SJ. 2003. Class III β-tubulin isotype: A key cytoskeletal protein at the crossroads of developmental neurobiology and tumor neuropathology. J. Child Neurol. 18:851–866.

Khoshnood N, Zamanian A. 2020. A comprehensive review on scaffold-free bioinks for bioprinting. Bioprinting 19.

Kim H, Park HJ, Choi H, Chang Y, Park H, Shin J, Kim Junyeop, Lengner CJ, Lee YK, Kim Jongpil. 2019. Modeling G2019S-LRRK2 Sporadic Parkinson's Disease in 3D Midbrain Organoids. Stem Cell Reports 12:518–531.

Kleinman HK, McGarvey ML, Liotta LA, Robey PG, Tryggvason K, Martin GR. 1982. Isolation and Characterization of Type IV Procollagen, Laminin, and Heparan Sulfate Proteoglycan from the EHS Sarcoma. Biochemistry 21:6188–6193.

Knight CG, Morton LF, Peachey AR, Tuckwell DS, Farndale RW, Barnes MJ. 2000. The collagen-binding a-domains of integrins α1/β1 and α2/β1 recognize the same specific amino acid sequence, GFOGER, in native (triple- helical) collagens. J. Biol. Chem. 275:35–40.

Knott EP, Assi M, Pearse DD. 2014. Cyclic AMP signaling: A molecular determinant of peripheral nerve regeneration. Biomed Res. Int. 2014.

Ko KR, Tam NW, Teixeira AG, Frampton JP. 2020. SH-SY5Y and LUHMES cells display differential sensitivity to MPP+, tunicamycin, and epoxomicin in 2D and 3D cell culture. Biotechnol. Prog. 36.

Kolesky DB, Truby RL, Gladman AS, Busbee TA, Homan KA, Lewis JA. 2014. 3D Bioprinting of Vascularized , Heterogeneous Cell-Laden Tissue Constructs. :3124–3130.

Kruse SA, Rose GH, Glaser KJ, Manduca A, Felmlee JP, Jack CR, Ehman RL. 2008. Magnetic resonance elastography of the brain. Neuroimage 39:231–237.

Lancaster MA, Renner M, Martin CA, Wenzel D, Bicknell LS, Hurles ME, Homfray T, Penninger JM, Jackson AP, Knoblich JA. 2013. Cerebral organoids model human brain development and

microcephaly. Nature 501:373–379.

Lavrentieva A, Kirsch M, Birnstein L, Pepelanova I, Handke W, Rach J, Seltsam A, Scheper T. 2019. Gelatin-methacryloyl (GelMA) formulated with human platelet lysate supports mesenchymal stem cell proliferation and differentiation and enhances the hydrogel's mechanical properties. Bioengineering 6.

Levato R, Jungst T, Scheuring RG, Blunk T, Groll J, Malda J. 2020. From Shape to Function: The Next Step in Bioprinting. Adv. Mater. 32.

Levato R, Lim KS, Li W, Asua AU, Peña LB, Wang M, Falandt M, Bernal PN, Gawlitta D, Zhang YS, et al. 2021. High-resolution lithographic biofabrication of hydrogels with complex microchannels from low-temperature-soluble gelatin bioresins. Mater. Today Bio 12:1–13.

Lew M. 2007. Overview of Parkinson ' s Disease.

Li X, Chen S, Li J, Wang X, Zhang J, Kawazoe N, Chen G. 2016. 3D culture of chondrocytes in gelatin hydrogels with different stiffness. Polymers (Basel). 8.

Magliaro C, Mattei G, Iacoangeli F, Corti A, Piemonte V, Ahluwalia A. 2019. Oxygen consumption characteristics in 3D constructs depend on cell density. Front. Bioeng. Biotechnol. 7:1–9.

Malda J, Visser J, Melchels FP, Jüngst T, Hennink WE, Dhert WJA, Groll J, Hutmacher DW. 2013. 25th anniversary article: Engineering hydrogels for biofabrication. Adv. Mater. 25:5011–5028.

Mattei G, Giusti S, Ahluwalia A. 2014. Design criteria for generating physiologically relevant in vitro models in bioreactors. Processes 2:548–569.

McCormack A, Highley CB, Leslie NR, Melchels FPW. 2020. 3D Printing in Suspension Baths: Keeping the Promises of Bioprinting Afloat. Trends Biotechnol. 38:584–593.

Mũnoz Z, Shih H, Lin CC. 2014. Gelatin hydrogels formed by orthogonal thiol-norbornene photochemistry for cell encapsulation. Biomater. Sci. 2:1063–1072.

Ou Z, Pan J, Tang S, Duan D, Yu D, Nong H, Wang Z. 2021. Global Trends in the Incidence, Prevalence, and Years Lived With Disability of Parkinson's Disease in 204 Countries/Territories From 1990 to 2019. Front. Public Heal. 9.

Ouyang L, Yao R, Zhao Y, Sun W. 2016. Effect of bioink properties on printability and cell viability for 3D bioplotting of embryonic stem cells. Biofabrication 8:1–12.

Peppas NA, Hilt JZ, Khademhosseini A, Langer R. 2006. Hydrogels in biology and medicine: From molecular principles to bionanotechnology. Adv. Mater. 18:1345–1360.

Prendergast ME, Burdick JA. 2021. Computational Modeling and Experimental Characterization of Extrusion Printing into Suspension Baths. Adv. Healthc. Mater.

Qiu B, Bessler N, Figler K, Buchholz MB, Rios AC, Malda J, Levato R, Caiazzo M. 2020. Bioprinting Neural Systems to Model Central Nervous System Diseases. Adv. Funct. Mater. 30.

Ray Dorsey E, Elbaz A, Nichols E, Abd-Allah F, Abdelalim A, Adsuar JC, Ansha MG, Brayne C, Choi JYJ, Collado-Mateo D, et al. 2018. Global, regional, and national burden of Parkinson's disease, 1990–

2016: a systematic analysis for the Global Burden of Disease Study 2016. Lancet Neurol. 17:939–953.

Rutishauser U. 1993. Adhesion molecules of the nervous system. Curr. Opin. Neurobiol. 3:709–715.

Scholz D, Pöltl D, Genewsky A, Weng M, Waldmann T, Schildknecht S, Leist M. 2011. Rapid, complete and large-scale generation of post-mitotic neurons from the human LUHMES cell line. J. Neurochem. 119:957–971.

Schuurman W, Levett PA, Pot MW, van Weeren PR, Dhert WJA, Hutmacher DW, Melchels FPW, Klein TJ, Malda J. 2013. Gelatin-methacrylamide hydrogels as potential biomaterials for fabrication of tissue-engineered cartilage constructs. Macromol. Biosci. 13:551–561.

Schwab A, Levato R, D'Este M, Piluso S, Eglin D, Malda J. 2020. Printability and Shape Fidelity of Bioinks in 3D Bioprinting. Chem. Rev. 120:11028–11055.

Shin SR, Bae H, Cha JM, Mun JY, Chen YC, Tekin H, Shin H, Farshchi S, Dokmeci MR, Tang S, et al. 2012. Carbon nanotube reinforced hybrid microgels as scaffold materials for cell encapsulation. ACS Nano 6:362–372.

Slater K, Partridge J, Nandivada H. 2018. Tuning the Elastic Moduli of Corning ® Matrigel ® and Collagen I 3D Matrices by Varying the Protein Concentration Application Note. 1:1–8.

Smirnova L, Harris G, Delp J, Valadares M, Pamies D, Hogberg HT, Waldmann T, Leist M, Hartung T. 2016. A LUHMES 3D dopaminergic neuronal model for neurotoxicity testing allowing long-term exposure and cellular resilience analysis. Arch. Toxicol. 90:2725–2743.

Srikanth P, Young-Pearse TL. 2014. Stem cells on the brain: Modeling neurodevelopmental and neurodegenerative diseases using human induced pluripotent stem cells. J. Neurogenet. 28:5–29.
Taylor Z, Miller K. 2004. Reassessment of brain elasticity for analysis of biomechanisms of hydrocephalus. J. Biomech. 37:1263–1269.

Theka I, Caiazzo M, Dvoretskova E, Leo D, Ungaro F, Curreli S, Managò F, Dell'Anno MT, Pezzoli G, Gainetdinov RR, et al. 2013. Rapid Generation of Functional Dopaminergic Neurons From Human Induced Pluripotent Stem Cells Through a Single-Step Procedure Using Cell Lineage Transcription Factors. Stem Cells Transl. Med. 2:473–479.

Thomas M, Willerth SM. 2017. 3-D bioprinting of neural tissue for applications in cell therapy and drug screening. Front. Bioeng. Biotechnol. 5:1–11.

Tong X jie, Hirai KI, Shimada H, Mizutani Y, Izumi T, Toda N, Yu P. 1994. Sciatic nerve regeneration navigated by laminin-fibronectin double coated biodegradable collagen grafts in rats. Brain Res.

Wei Z, Lin B, Chen T, Daie K, Svoboda K, Druckmann S. 2020. A comparison of neuronal population dynamics measured with calcium imaging and electrophysiology. PLoS Comput. Biol. 16:1–29.

Yue K, Trujillo-de Santiago G, Alvarez MM, Tamayol A, Annabi N, Khademhosseini A. 2015. Synthesis, properties, and biomedical applications of gelatin methacryloyl (GelMA) hydrogels. Biomaterials 73:254–271.

Zhou X, Cui H, Nowicki M, Miao S, Lee SJ, Masood F, Harris BT, Zhang LG. 2018. Three-Dimensional-Bioprinted Dopamine-Based Matrix for Promoting Neural Regeneration. ACS Appl. Mater. Interfaces 10:8993–9001.

Supplementary Figures

2.1.2 Microparticle size

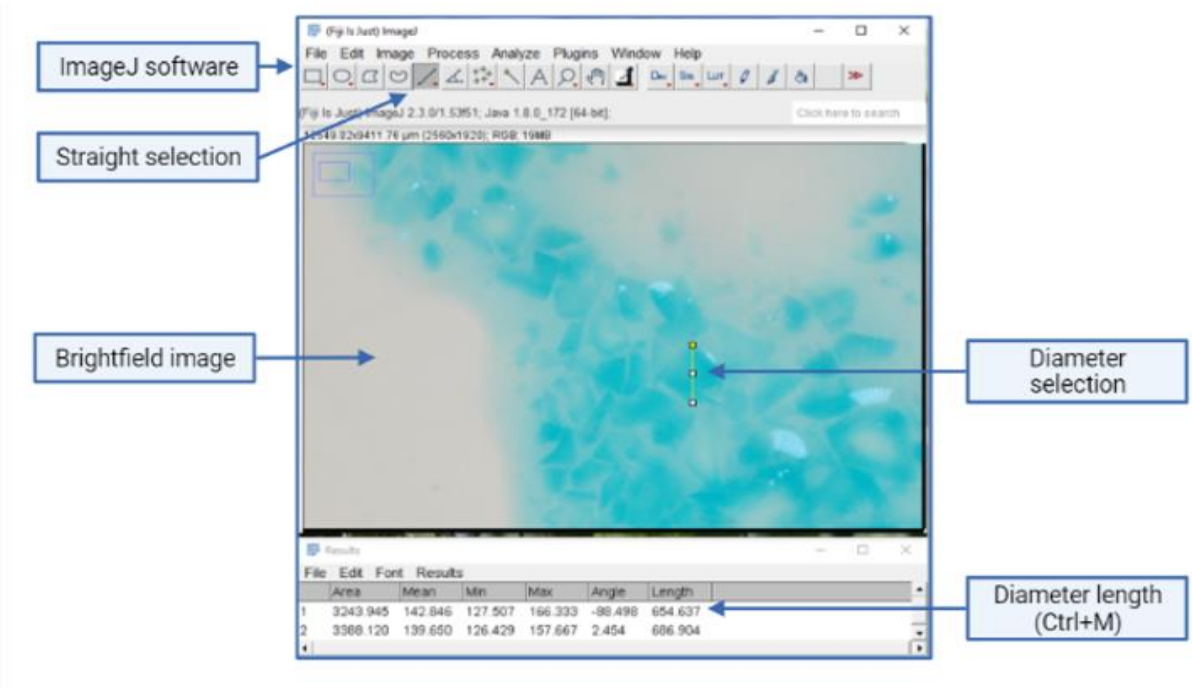

Supplementary Fig. S1. Screenshot of ImageJ Software showing an uploaded brightfield image of milled GelMA microparticles. The straight line selection is used to measure the diameter length (Analysis – Measure (Ctrl+M)).

2.3 3D bioprinting process

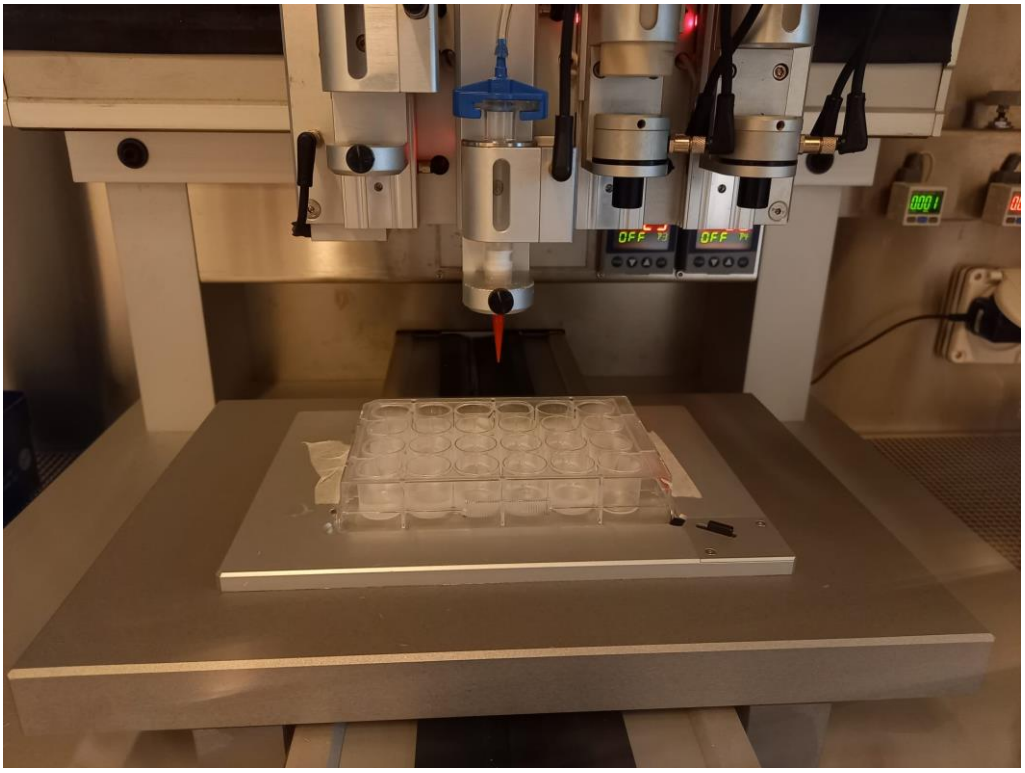

Supplementary Fig. S2. Set-up for the printing process when a 24-wells plate is used.

2.3.3 printing LUHMES

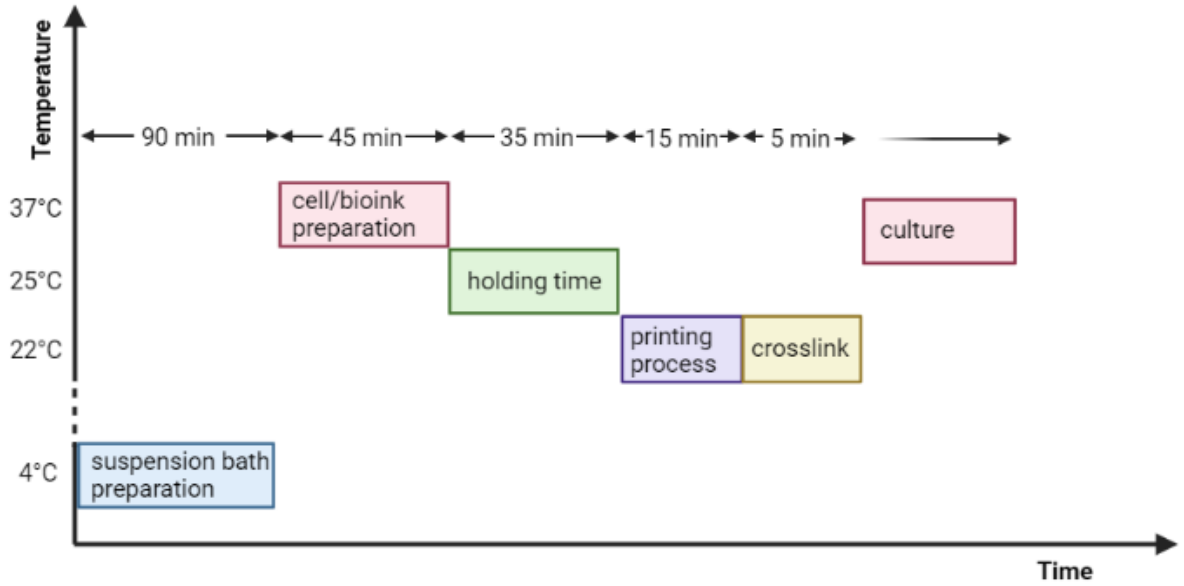

Supplementary Fig. S3. Schematic of the experiment indicating the timing and temperature of different parts of the biofabrication process.

2.4 Cell Viability Assays to determine Printing Resolution and Filament Width

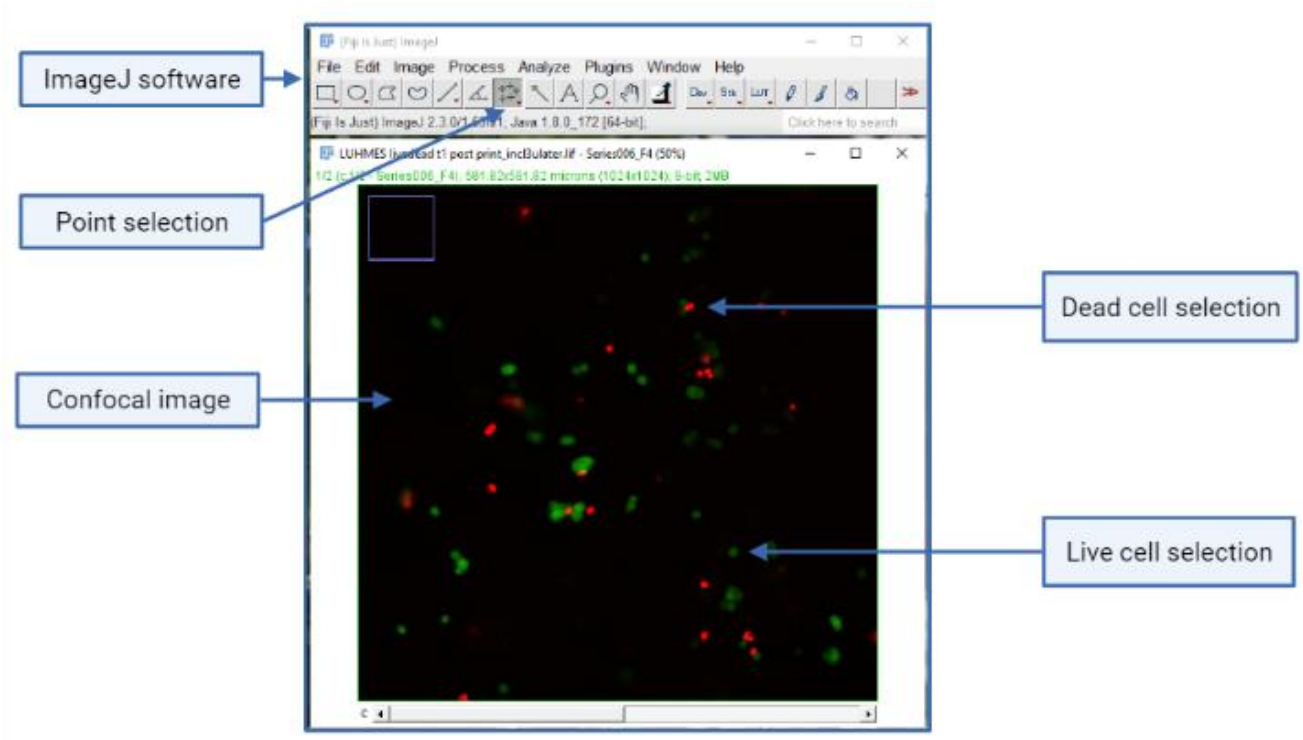

Supplementary Fig. S4. Screenshot of ImageJ Software showing an uploaded Confocal microscopy image of live and dead LUHMES cells. Cell viability was quantified after splitting the red and green channels and counting cells by point selection.

3.1.2 Milling for 60s results in the optimal microparticle slurry

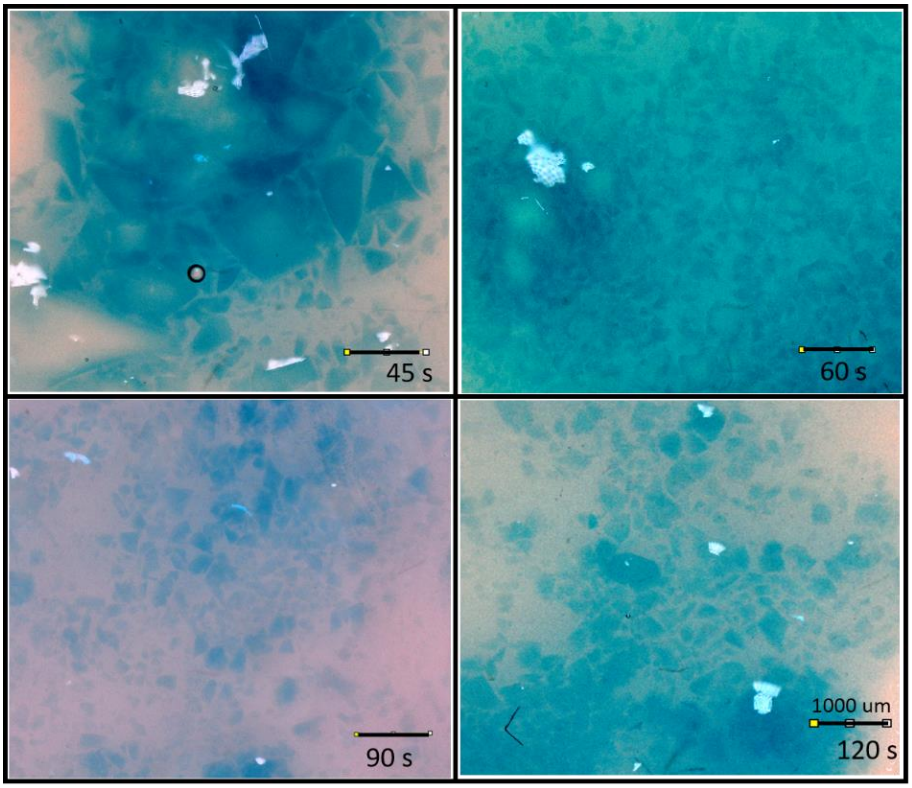

Supplementary Fig. S5. Representative images of GelMA microparticles produced by blending for 45s, 60s, 90s, and 120s.

3.1.4 Swelling Properties of 5% milled and bulk GelMA are comparable

condition	#	mwet,t0	mdry,t0	mswollen,t1	mdry,t1	sol fraction	swelling ratio
5% bulk	1	0,4307	0,0158	0,1628	0,0117	25,9494	13,9145
5% bulk	2	0,5124	0,0154	0,1545	0,0114	25,9740	13,5526
5% bulk	3	0,4894	0,0158	0,1664	0,0121	23,4177	13,7521
5% blended	4	0,3196	0,0150	0,1374	0,0114	24,0000	12,0526
5% blended	5	0,3341	0,0148	0,1433	0,0122	17,5676	11,7459
5% blended	6	0,3264	0,0153	0,1408	0,0107	30,0654	13,1589

Supplementary Fig. S6. Values to calculate the sol fraction and swelling ratio. It can be noted that the milled GelMA samples are lighter, because they crosslink less around the edges of the mold and are thus somewhat smaller compared to the full size bulk GelMA discs.

Appendix

2.1.3 Mechanical Testing

Stress-Relaxation and Compression Protocol

- Book the dynamic mechanical analyzer (DMA Q800, TA instruments, The Netherlands), located at the David de Wiedgebouw, room 3.34
- Open TA Instruments on the computer and select DMA Q800.
- Calibrate the clamp. Select compression, click next, ignore open furnace, calibrate 0 position.
- Change the settings on the summary or load the procedure template:
    - Mode: DMA controlled force
    - Test: custom
    - Clamp: compression
    - Sample shape: round disk
    - Put first dimension at 0, second will be the measured diameter of your sample
- Change sample name and create a new data file
- Change settings in the procedure tab:
    - Compression:
        - Ramp force: 0.1N/min to 0.2N (2 mins)
        - Data sampling interval: 0.1 s/p
        - Min. force 0.0001N
        - Preload force 0.001N
    - Stress-relaxation
        - Maximum 0.004N
        - Strain 10%
        - 2 min stress, 1 min recovery
- Change name in the notes tab, check Poisson's ratio
- Then apply all changes, check for a green diamond next to "Run"
- Measure height using the ruler symbol
- Once completed, run the protocol (green play icon)
- Wait until the run is completed (marked in red)
- Change graph according to wishes, e.g. X: Time, Y: Strain or Displacement
- To analyze: open file using TA analyzer, check that the signals are correct
- Go to view: data table – report, increment for data points: 0.01min
- Copy and paste results in excel file using wizard to separate into columns
- Analyze data, calculate Young's modulus as the slope of the line during the linear phase
    - area=$\pi * r^2$
    - stress= static force/area
    - strain = -displacement/(height*1000)
    - make a graph, x = strain, y = stress
    - calculate linear slope from 0.05-0.15 strain (5-15%)
- Calculate the Elasticity
    - f1= highest value
    - f2= value at 2 mins (when recovery starts)
    - Elasticity= (f2/f1)*100

2.2 Cell Culture Media

Cell type	Medium	Supplements	Transcription factors and molecules
hiMSCs	α-MEM	10% (v/v) FBS 1% (v/v) Penstrep 1% (v/v) AsAP 0.1% (v/v) bFGF	
hESC	Stemflex		
LUHMES regular expansion medium	LUHMES growth medium	1% (v/v) Penstrep	
LUHMES differentiation medium	LUHMES growth medium	1% (v/v) Penstrep	Dox AsAP GDNF BDNF Db-cAMP

2.2.3 Differentiation medium LUHMES

	Stock	Conc.	1 ml medium	Conc. for total volume	1ml medium*
dox	2 mg/ml	1ug/ml	0.5 µl	1ug/ml	1 µl
GDNF	20 ug/ml	2 ng/ml	0.1 µl	2 ng/ml	0.2 µl
BDNF	20 ug/ml	2 ng/ml	0.1 µl	2 ng/ml	0.2 µl
AsAP	20 mM	0.2 mM	20 µl	0.2 mM	40 µl
Db-cAMP	50 mM	1 mM	40 µl	1 mM	80 µl

** Assuming total volume = 1x volume sample + 1x volume medium*

2.3 3D bioprinting process

G-Code for RegenHU 3D Discovery – 24 wells plate

```
(RegenHU)
(File: 24Well_Mshape_CORNING_adjusted)
(Date : 07.10.2021)

(Program-Start)
G90 G94          ; G90 FOR ABSOLUTE COORDINATES, FEEDRATE AS MM/MINUTE

G76 Z0
M99              ; AIR PRESSURE ON
M90 P2 D1
M95 P2           ; SELECT PRINTHEAD

G0 X-53 Y25      ; A ONE, MOVE TO COORDINATE AT MAX SPEED
G0 Z0
M97              ; START EXTRUDING
F3               ; FEEDRATE
```

```
G1 X-53 Y25     ; LINEAR MOTION TO COORDINATE AT SPEED DEFINED BY F
X-53 Y30
X-51 Y30
X-51 Y25
X-48 Y25
X-48 Y30
X-44 Y30
X-44 Y25
M96             ; STOP EXTRUDING
G0 Z25          ; LIFT PRINTHEAD

G0 X-53 Y6      ; B ONE
G0 Z0
M97
G1 X-53 Y6
X-53 Y11
X-51 Y11
X-51 Y6
X-48 Y6
X-48 Y11
X-44 Y11
X-44 Y6
M96
G0 Z25

G0 X-53 Y-14    ; C ONE
G0 Z0
M97
G1 X-53 Y-9
X-51 Y-9
X-51 Y-14
X-48 Y-14
X-48 Y-9
X-44 Y-9
X-44 Y-14
M96
G0 Z25

G0 X-53 Y-32    ; D ONE
G0 Z0
M97
G1 X-53 Y-27
X-51 Y-27
X-51 Y-32
X-48 Y-32
X-48 Y-27
X-44 Y-27
X-44 Y-32
M96
G0 Z25

G0 X-33.5 Y25   ; A TWO
```

```
G0 Z0
M97
F2
G1 X-33.5 Y30
X-31.5 Y30
X-31.5 Y25
X-28.5 Y25
X-28.5 Y30
X-24.5 Y30
X-24.5 Y25
M96
G0 Z25

G0 X-33.5 Y5     ; B TWO
G0 Z0
M97
F2
G1 X-33.5 Y10
X-31.5 Y10
X-31.5 Y5
X-28.5 Y5
X-28.5 Y10
X-24.5 Y10
X-24.5 Y5
M96
G0 Z25

G0 X-33.5 Y-14  ; C TWO
G0 Z0
M97
F2
G1 X-33.5 Y-9
X-31.5 Y-9
X-31.5 Y-14
X-28.5 Y-14
X-28.5 Y-9
X-24.5 Y-9
X-24.5 Y-14
M96
G0 Z25

G0 X-33.5 Y-32  ; D TWO
G0 Z0
M97
F2
G1 X-33.5 Y-27
X-31.5 Y-27
X-31.5 Y-32
X-28.5 Y-32
X-28.5 Y-27
X-24.5 Y-27
X-24.5 Y-32
```

```
M96
G0 Z25


G0 X-14 Y25      ; A THREE
G0 Z0
M97
F2
G1 X-14 Y30
X-12 Y30
X-12 Y25
X-9 Y25
X-9 Y30
X-5 Y30
X-5 Y25
M96
G0 Z25

G0 X-14 Y5       ; B THREE
G0 Z0
M97
F2
G1 X-14 Y10
X-12 Y10
X-12 Y5
X-9 Y5
X-9 Y10
X-5 Y10
X-5 Y5
M96
G0 Z25

G0 X-14 Y-14     ; C THREE
G0 Z0
M97
F2
G1 X-14 Y-9
X-12 Y-9
X-12 Y-14
X-9 Y-14
X-9 Y-9
X-5 Y-9
X-5 Y-14
M96
G0 Z25

G0 X-14 Y-32     ; D THREE
G0 Z0
M97
F2
G1 X-14 Y-27
X-12 Y-27
```

```
X-12 Y-32
X-9 Y-32
X-9 Y-27
X-5 Y-27
X-5 Y-32
M96
G0 Z25

G0 X5 Y25          ; A FOUR
G0 Z0
M97
F2
G1 X5 Y30
X7 Y30
X7 Y25
X10 Y25
X10 Y30
X14 Y30
X14 Y25
M96
G0 Z25

G0 X5 Y5           ; B FOUR
G0 Z0
M97
F2
G1 X5 Y10
X7 Y10
X7 Y5
X10 Y5
X10 Y10
X14 Y10
X14 Y5
M96
G0 Z25

G0 X5 Y-14         ; C FOUR
G0 Z0
M97
F2
G1 X5 Y-9
X7 Y-9
X7 Y-14
X10 Y-14
X10 Y-9
X14 Y-9
X14 Y-14
M96
G0 Z25

G0 X5 Y-32         ; D FOUR
G0 Z0
```

```
M97
F2
G1 X5 Y-27
X7 Y-27
X7 Y-32
X10 Y-32
X10 Y-27
X14 Y-27
X14 Y-32
M96
G0 Z25

G0 X24 Y25      ; A FIVE
G0 Z0
M97
F2
G1 X24 Y30
X26 Y30
X26 Y25
X29 Y25
X29 Y30
X33 Y30
X33 Y25
M96
G0 Z25

G0 X24 Y5       ; B FIVE
G0 Z0
M97
F2
G1 X24 Y10
X26 Y10
X26 Y5
X29 Y5
X29 Y10
X33 Y10
X33 Y5
M96
G0 Z25

G0 X24 Y-14     ; C FIVE
G0 Z0
M97
F2
G1 X24 Y-9
X26 Y-9
X26 Y-14
X29 Y-14
X29 Y-9
X33 Y-9
X33 Y-14
M96
```

```
G0 Z25

G0 X24 Y-32       ; D FIVE
G0 Z0
M97
F2
G1 X24 Y-27
X26 Y-27
X26 Y-32
X29 Y-32
X29 Y-27
X33 Y-27
X33 Y-32
M96
G0 Z25

G0 X44 Y25        ; A SIX
G0 Z0
M97
F2
G1 X44 Y30
X46 Y30
X46 Y25
X49 Y25
X49 Y30
X53 Y30
X53 Y25
M96
G0 Z25

G0 X44 Y5         ; B SIX
G0 Z0
M97
G1 X44 Y10
X46 Y10
X46 Y5
X49 Y5
X49 Y10
X53 Y10
X53 Y5
M96
G0 Z25

G0 X44 Y-14       ; C SIX
G0 Z0
M97
G1 X44 Y-9
X46 Y-9
X46 Y-14
X49 Y-14
X49 Y-9
X53 Y-9
```

```
X53 Y-14
M96
G0 Z25

G0 X44 Y-32     ; D SIX
G0 Z0
M97
G1 X44 Y-27
X46 Y-27
X46 Y-32
X49 Y-32
X49 Y-27
X53 Y-27
X53 Y-32
M96             ; STOP EXTRUDING
G0 Z25
M98             ; CALL SUB PROGRAM

(Program-End)
G76 Z0
G0 X0 Y0        ; MOVE PRINTHEAD BACK TO ORIGIN
M2              ; END OF PROGRAM
```

G-Code for RegenHU 3D Discovery – 48 wells plate

```
(RegenHU)
(File: 48Well_snake_cellstar/greiner)
(Date : 02.12.2021)

(Program-Start)
G90 G94         ; G90 FOR ABSOLUTE COORDINATES, FEEDRATE AS MM/MINUTE

G76 Z0
M99             ; AIR PRESSURE ON
M90 P2 D1
M95 P2          ; SELECT PRINTHEAD

G0 X-47.5 Y35   ; A ONE, MOVE TO COORDINATE AT MAX SPEED
G0 Z0
M97             ; START EXTRUDING
F3              ; FEEDRATE
G1 X-47.5 Y35   ; LINEAR MOTION TO COORDINATE AT SPEED DEFINED BY F
X-47.5 Y30
X-45.5 Y30
X-45.5 Y35
X-42.5 Y35
X-42.5 Y30
M96             ; STOP EXTRUDING
G0 Z25          ; LIFT PRINTHEAD


G0 X-47.5 Y22   ; B ONE
```

```
G0 Z0
M97             ; START EXTRUDING
F3              ; FEEDRATE
G1 X-47.5 Y22
X-47.5 Y17
X-45.5 Y17
X-45.5 Y22
X-42.5 Y22
X-42.5 Y17
M96             ; STOP EXTRUDING
G0 Z25


G0 X-47.5 Y9    ; C ONE
G0 Z0
M97             ; START EXTRUDING
F3              ; FEEDRATE
G1 X-47.5 Y9
X-47.5 Y4
X-45.5 Y4
X-45.5 Y9
X-42.5 Y9
X-42.5 Y4
M96             ; STOP EXTRUDING
G0 Z25


G0 X-34.5 Y35   ; A TWO
G0 Z0
M97             ; START EXTRUDING
F4              ; FEEDRATE
G1 X-34.5 Y35
X-34.5 Y30
X-32.5 Y30
X-32.5 Y35
X-29.5 Y35
X-29.5 Y30
M96             ; STOP EXTRUDING
G0 Z25


G0 X-34.5 Y22   ; B TWO
G0 Z0
M97             ; START EXTRUDING
F4              ; FEEDRATE
G1 X-34.5 Y22
X-34.5 Y17
X-32.5 Y17
X-32.5 Y22
X-29.5 Y22
X-29.5 Y17
M96             ; STOP EXTRUDING
```

```
G0 Z25

G0 X-34.5 Y9    ; C TWO
G0 Z0
M97             ; START EXTRUDING
F4              ; FEEDRATE
G1 X-34.5 Y9
X-34.5 Y4
X-32.5 Y4
X-32.5 Y9
X-29.5 Y9
X-29.5 Y4
M96             ; STOP EXTRUDING
G0 Z25


G0 X-21.5 Y35   ; A THREE
G0 Z0
M97             ; START EXTRUDING
F5              ; FEEDRATE
G1 X-21.5 Y35
X-21.5 Y30
X-19.5 Y30
X-19.5 Y35
X-16.5 Y35
X-16.5 Y30
M96             ; STOP EXTRUDING
G0 Z25


G0 X-21.5 Y22   ; B THREE
G0 Z0
M97             ; START EXTRUDING
F5              ; FEEDRATE
G1 X-21.5 Y22
X-21.5 Y17
X-19.5 Y17
X-19.5 Y22
X-16.5 Y22
X-16.5 Y17
M96             ; STOP EXTRUDING
G0 Z25


G0 X-21.5 Y9    ; C THREE
G0 Z0
M97             ; START EXTRUDING
F5              ; FEEDRATE
G1 X-21.5 Y9
X-21.5 Y4
X-19.5 Y4
X-19.5 Y9
```

```
X-16.5 Y9
X-16.5 Y4
M96             ; STOP EXTRUDING
G0 Z25


G0 X-8.5 Y35    ; A FOUR
G0 Z0
M97             ; START EXTRUDING
F6              ; FEEDRATE
G1 X-8.5 Y35
X-8.5 Y30
X-6.5 Y30
X-6.5 Y35
X-3.5 Y35
X-3.5 Y30
M96             ; STOP EXTRUDING
G0 Z25


G0 X-8.5 Y22    ; B FOUR
G0 Z0
M97             ; START EXTRUDING
F6              ; FEEDRATE
G1 X-8.5 Y22
X-8.5 Y17
X-6.5 Y17
X-6.5 Y22
X-3.5 Y22
X-3.5 Y17
M96             ; STOP EXTRUDING
G0 Z25


G0 X-8.5 Y9     ; C FOUR
G0 Z0
M97             ; START EXTRUDING
F6              ; FEEDRATE
G1 X-8.5 Y9
X-8.5 Y4
X-6.5 Y4
X-6.5 Y9
X-3.5 Y9
X-3.5 Y4
M96             ; STOP EXTRUDING
G0 Z25

M98             ; CALL SUB PROGRAM

G76 Z0
G0 X0 Y0        ; MOVE PRINTHEAD BACK TO ORIGIN
M2              ; END OF PROGRAM
```